Debris Disks: Structure and Composition

A. Meredith Hughes,[1] Gaspard Duchêne,[2,3] Brenda C. Matthews[4,5]

[1]Wesleyan
[2] Astronomy Department, Univeristy of California Berkeley, Berkeley CA 94720-3411, USA
[3] Université Grenoble Alpes, CNRS, Institut d'Astrophysique et de Planétologie de Grenoble, Grenoble 38000, France
[4] Herzberg Astronomy & Astrophysics Programs, National Research Council of Canada, 5071 West Saanich Road, Victoria, BC, V9E 2E7, Canada
[5] Department of Physics & Astronomy, University of Victoria, 3800 Finnerty Road, Victoria, BC, V8P 5C2, Canada

Xxxx. Xxx. Xxx. Xxx. YYYY. AA:1–59

https://doi.org/10.1146/((please add article doi))

Keywords

keywords, separated by comma, no full stop, lowercase

Abstract

Abstract text, approximately 150 words.

Contents

1. Introduction 3
   1.1. What is a Debris Disk? 3
   1.2. Observations of Debris Disks 4
   1.3. Scope of this review 6
2. Demographics 7
   2.1. Kuiper Belt Analogues 7
   2.2. Two Temperature Disks 8
   2.3. Exododis 9
   2.4. Correlations with Planetary Systems 11
3. Dust properties 13
   3.1. Spatially unresolved observations 13
   3.2. Spatially resolved observations 14
   3.3. Global analyses 19
4. Outer Disk Structure 21
   4.1. Diversity of Resolved Structures 22
5. Planet-Disk Interaction 32
   5.1. RV Planets with Debris Disks Much Farther Out 32
   5.2. Direct Observations of Planet-Disk Interaction 33
6. Variability in Debris Disks 36
   6.1. Detections in Stellar Spectra 36
   6.2. Detection in Light Curves of Circumstellar Dust 36
   6.3. Detectability in Stellar Light Curves 37
   6.4. Directly Imaged Features 38
7. Gas in Debris Disks 40
   7.1. Overview and demographics of gas-bearing debris disks 40
   7.2. Composition of Atomic Gas 44
   7.3. Molecular Gas: Quantity, Spatial Distribution, and Composition 46
   7.4. Origin 49

1. Introduction

1.1. What is a Debris Disk?

Flattened disks of gas and dust are a ubiquitous outcome of the star formation process, and an integral component of the formation of planetary systems. The formation of stars and planets are inextricably linked, and systems go through a number of distinct stages as they evolve from overdense cores in massive molecular clouds to mature planetary systems (see, e.g., Shu et al. 1987; Li et al. 2014, and references therein). The initial dense core collapses under the influence of gravity to form a protostar embedded in a molecular envelope, while material falls from the envelope onto a forming pseudodisk, perhaps launching an outflow to help dissipate immense quantities of angular momentum. The envelope ultimately dissipates and the disk settles into regular Keplerian motion, leaving behind a protoplanetary (or planet-forming) disk of gas and dust composed of the leftover material from the formation of the star – which is by this stage a pre-main sequence star. Eventually the predominantly primordial material from the protoplanetary disk dissipates through some combination of stellar and planetary mechanisms involving accretion, photoevaporation, and winds (see, e.g., Williams & Cieza 2011; Alexander et al. 2014; Wyatt et al. 2015; Ercolano & Pascucci 2017, and references therein). Beyond that point, the luminosity of the dusty disk drops precipitously and any remaining dust is believed to be second-generation material from collisions between Pluto-like planetesimals (since its lifetime due to radiation pressure is shorter than the age of the star), and is therefore called a "debris" disk.

Debris disks are common; they are detected around at least $\sim 25\%$ of main sequence A stars (Thureau et al. 2014) and $\sim 20\%$ of Solar-type stars (Montesinos et al. 2016; Eiroa et al. 2013) with variations over spectral classes (Sibthorpe et al. 2017). The occurrence fraction is necessarily a lower limit, due to the finite sensitivity of our detectors. Our own Solar System contains not one, but two debris disks: the zodiacal light, which can be seen with the naked eye from dark-sky locations on Earth and is composed primarily of material from collisions between Jupiter-family comets in the inner Solar System, and the Kuiper belt. While the zodiacal light appears brighter from Earth since we are sitting inside it, the Kuiper belt would appear brighter to a distant alien astronomer due to the greater mass and corresponding total surface area of the dust. Neither debris disk would be detectable around a neighboring star using current technology; our own Solar System's debris belts are still 1-2 orders of magnitude too faint to be observed with current instrumentation. All debris disks currently detected around other stars are therefore scaled-up versions of those found in our own planetary system, and we expect that debris disks are far more common than the detected fraction – at least as common as the planetary systems that have been found to be ubiquitous throughout the galaxy.

While protoplanetary disks and debris disks are distinct evolutionary stages (with some blurring at the boundary), it is not trivial to distinguish between the two. Various criteria have been proposed in the literature, but nearly all rules either have clear exceptions or rely heavily on assumptions about poorly constrained properties of the system. Age is not a good criterion since stellar clusters with ages of $\sim$5-15 Myr contain coexisting examples of both protoplanetary and debris disks, and even clusters as young as 2-3 Myr show signs of incipient debris disks Espaillat et al. (2017). Similarly, the presence of molecular gas is not a good criterion since many debris disks exhibit gas emission. The most practical criterion seems to be optical depth: the dust in debris disks is optically thin across the electromagenetic spectrum, while the dust in protoplanetary disks is typically extremely

optically thick at optical wavelengths and may remain optically thick in the inner regions even into the millimeter part of the spectrum. The observational proxy most frequently used to estimate optical depth is the fractional excess luminosity in the infrared $\tau = L_{IR}/L_{bol}$, or more directly, the ratio of the disk flux to the stellar flux at a particular infrared wavelength. In this review, we adopt a cutoff of $\tau < 8 \times 10^{-3}$ to define a debris disk, selected somewhat arbitrarily to place HD 141569 right on the boundary, since it seems to be the best candidate for a truly intermediate object between the protoplanetary and debris disk phase (Wyatt et al. 2015).

1.2. Observations of Debris Disks

GD: Some of the material here is somewhat redundant with what is in other sections, particularly the dust section. While I think it's a good idea to have the top-level ideas up front in the introduction, I'd suggest that we trim down a lot of the details (for instance: the equations related to MBB models, as well as that describing the connection between α_{mm} and β) away from this section.

There are many different ways of observing a debris disk. Images can reveal the morphology of both gas and dust emission, and dust emission can be imaged across the electromagnetic spectrum to reveal thermal emission as well as scattered light. The broad-band Spectral Energy Distribution (SED) is the primary diagnostic used to separate the starlight from the disk excess, and to characterize the fractional excess luminosity of the system (i.e., the amount of emission reprocessed by the disk, which appears in excess of the stellar photosphere). The long-wavelength slope of the spectral energy distribution is often used as a diagnostic that can be related to the basic properties of the grain size distribution (see, e.g., Ricci et al. 2015b; MacGregor et al. 2016b, and references therein). In addition to the dust, there is occasionally a molecular gas component that can be detected either through emission or absorption spectroscopy (see Section 7 for more detail). Here we sketch out a few basic concepts that are important for understanding debris disk observations and comparing results between different methods.

(Modified) Blackbody SED Fitting — The complexity of the approach taken to modeling a debris disk SED depends to some extent on how well sampled the SED is. When only a few photometric data points are measured, and when those points are confined primarily to the infrared, many disks are well described by a single blackbody added to the photosphere (in general simple sums of disk and star models are appropriate for debris disks since the optical depth of the dust is low). With finer sampling of the infrared SED, for example systems for which a *Spitzer* IRS spectrum is available, often multiple components with different temperatures are required to fit the SED data (see, e.g., Ballering et al. 2013; Chen et al. 2014; Pawellek et al. 2014). If the long-wavelength tail of the SED is sampled by at least a couple of photometric points, then it is typically necessary to model the emission with a modified blackbody that takes into account the decrease in emission/absorption efficiency Q at wavelengths longer than approximately $2\pi a$, where a is the radius of a dust grain. Some models include a sharp break with $Q = 1$ for wavelengths $< 2\pi a$ and $Q \propto \lambda^{-\beta}$ for wavelengths $\geq 2\pi a$, where β is a free parameter that describes the long-wavelength slope of the grain opacity spectrum. An elegant parameterization introduced by (Williams et al. 2004) introduces a smooth function with the appropriate asymptotic behavior to avoid the sharp discontinuity: $Q(\lambda) = 1 - \exp\left[-(2\pi a/\lambda)^{\beta}\right]$. SED fitting is often used to estimate the radius of a debris disk by connecting the temperature derived from the

(modified) blackbody fit to the SED to a radius by assuming either that the grains are in blackbody equilibrium with the central star or (more rarely) by assuming a composition and size distribution that allows the temperature to be related to the radius of the disk. As described in Section 2.4 below, resolved observations of debris disks generally find that the true radii are systematically larger than the radii derived from blackbody fitting, due to the presence of small grains in the disk that emit inefficiently at long wavelengths and therefore have temperatures greater than the blackbody equilibrium temperature.

Different Grain Sizes at Different Wavelengths — As imaging capabilities have improved across the electromagnetic spectrum, it has become possible to compare the spatial distribution of grains of different sizes within a single disk by making multiwavelength, spatially resolved observations of the disk. The rule of thumb is that the grain size that dominates the emission in an image at a given wavelength is approximately equal to the wavelength of observation. This rule of thumb is a balance between two trends working in opposite directions: on the one hand, the grain size distribution is heavily weighted towards small grains. The number of grains of a particular size, $N(a)$, depends on the size approximately as $dN/da \propto a^{-q}$. The exponent of this power law $q = 3.5$ is predicted by theory (Dohnanyi 1969; Pan & Schlichting 2012), and generally confirmed by observation (Ricci et al. 2015b; MacGregor et al. 2016b). The surface area capable of emitting is therefore heavily weighted towards smaller grains. On the other hand, dust grains only emit efficiently at wavelengths shorter than their physical size (which can be understood conceptually if the dust grains are imagined to be tiny antennas along which charge must oscillate to produce electromagnetic radiation: if the antenna is smaller than the wavelength of light, it cannot efficiently radiate). At wavelengths longer than their size, the emission efficiency drops steeply, roughly as $1/\lambda$. Therefore, at a given wavelength, only grains comparable to or larger than that wavelength can emit efficiently. But since the emitting area is weighted so heavily towards the smallest grains, the total emission is dominated by the smallest grains capable of emitting efficiently – namely, grains with sizes approximately equal to the wavelength of observation.

Spectral Index and Grain Size Distribution — When modified blackbodies or more complex calculated or tabulated opacities are used to fit the SED of a debris disk, one quantity of interest is the long-wavelength slope of the SED since it can be related to the slope of the grain size distribution in the disk. The millimeter spectral index $\alpha_{\rm mm}$ is defined as the power-law index describing the flux F_ν emitted by the disk as a function of frequency: $F_\nu \propto nu^{\alpha_{\rm mm}}$. Since the frequency dependence of the flux is determined by the product of the Planck function and the mass opacity, the grain size distribution power law q can be written as $(\alpha_{\rm mm} - \alpha_{\rm Planck})/\beta_s + 3$, where $\alpha_{\rm Planck}$ is 2 in the Rayleigh-Jeans limit and β_s is empirically determined to have a value 1.8 ± 0.2 (Draine 2006). Conceptually, this means that measuring the flux as a function of frequency tells us the number of dust grains as a function of grain size.

The overarching goal of modern studies of planet formation is to connect the initial conditions in a disk (gas and dust surface density, temperature, and velocity) to the final outcomes (exoplanet statistics), via models of planetary system formation and evolution. Historically, astronomers have tended to assume that protoplanetary disks provide information about the initial conditions, debris disks told us about orbital evolution during the "clean-up" phase at the end of oligarchic growth, and exoplanets told us about final configurations. The picture has become somewhat more complex recently, with mounting evidence that planets generally form quite early in the protoplanetary disk phase (e.g., ALMA Partnership et al. 2015) and that gas and dust in these systems are already significantly evolved

relative to ISM conditions (e.g., Williams & Cieza 2011, and references therein). However, it is still clear that some phases of evolution must take place during the debris disk phase. Debris disks also provide a unique opportunity to study directly imaged planets and disks in the same system, which is much more difficult in protoplanetary disks. Debris disks are also important because the secondary material of which they are composed (dust, and at least in some cases gas) can tell us about the composition of exoplanetary material, in a manner analogous to the way in which we learn about the interior of the earth from asteroid samples and meteorites.

1.3. Scope of this review

This review is focused on recent observational developments in understanding debris disk structure and evolution. There have been a number of notable advances in observational capability across the electromagnetic spectrum in recent years that have substantially enhanced our ability to spatially resolve debris disk structure at multiple wavelengths, yielding insight into the physical mechanisms shaping their evolution. Recent spatially resolved observations from facilities like *HST*, GPI, SPHERE, *Herschel*, and ALMA dominate the major results in this review. We approach the review from the observational direction, while pointing out ties to theory papers, which is intended to be in a complementary direction to other recent reviews (e.g., Wyatt 2008; Krist et al. 2010).

We have attempted to select topics without comprehensive recent reviews. For example, we provide only a brief update on debris disk demographics, since several recent major reviews have covered that area thoroughly (Wyatt 2008; Matthews et al. 2014b), addressing questions like the incidence of debris disks around stars of different ages and masses, and how debris disk incidence as a function of time connects to planet formation processes. We also limit the scope of this review to stars on the main sequence, since there are at least two comprehensive recent reviews of the rapidly developing field of debris disks around post-main sequence stars (Farihi 2016; Veras 2016).

Recently, the field has been moving away from statistics and more towards integrating our knowledge into understanding of underlying planetary system and its dynamics (including changes in the time domain). The major topics covered by this review include: a brief update on disk demographics in Section 2, an overview of the properties of dust largely informed by spectroscopy and polarimetric studies in Section 3, a summary of the structural diversity observed in outer disks as a result of high-resolution imaging across the electromagnetic spectrum in Section 4, a discussion of planet-disk interaction with particular emphasis on the growing subset of systems in which is is possible to obtain direct imaging of both disks and planets in the same system in Section 5, an exploration of the emerging field of time-domain studies of debris disk properties in Section 6, and finally, a comprehensive review of the atomic and molecular gas component of debris disks and our current understanding of its origin and composition in Section 7.

2. Demographics

Our understanding of the demographics of debris disks is driven by large surveys in the infrared where the disks are most readily detected through the presence of an "infrared excess" above the stellar photosphere, a signature of circumstellar dust. From their discovery with IRAS through the Spitzer, WISE and Herschel missions, hundreds of stars have been probed in young and nearby populations to gauge the incidence rate of infrared excess. The rates of incidence typically reported from surveys for debris signatures are in fact better termed detection rates. Inter-comparison of detection rates in different surveys is difficult since they often probe different regions of the disk, and the likelihood of detecting a debris disk around a nearby star depends on the wavelength and sensitivity of the observation as well as the inherent properties of the disk and the star it surrounds, including its distance. Even the characterization of the photosphere affects our ability to detect disks, since the typical means of identifying a disk in emission is the detect emission above the photospheric level. Wyatt (2008) and Matthews et al. (2014b) show figures illustrating the relative detectability of disks around stars of various spectral types.

2.1. Kuiper Belt Analogues

Many of the results of Spitzer and Herschel surveys to date were detailed in Matthews et al. (2014b); here we detail primarily new analyses undertaken since that review. The bulk of the demographics results from Herschel focus on the data taken by the DEBRIS and DUNES surveys at 100 and 160 μm toward samples of 446 A through M stars and 231 FGK stars, respectively, with significant overlap in their targets and observing strategy. Overall, the smallest dust fractional luminosities reached by the *Herschel* observations were an order of magnitude deeper than those attained by Spitzer, reaching within an order of magnitude of that of the Kuiper Belt (a few $\times 10^{-7}$, Vitense et al. 2012).

Analysis of data from these surveys has been compiled by various authors (Sierchio et al. 2014; Eiroa et al. 2013; Montesinos et al. 2016; Thureau et al. 2014; Sibthorpe et al. 2017) in addition to many more papers focusing on individual objects. Sibthorpe et al. (2017, submitted) present results from the Herschel DEBRIS survey sample of 275 FGK stars; this sample has significant overlap with the DUNES sample (Eiroa et al. 2013; Montesinos et al. 2016), but extends to larger volumes to capture the nearest $\sim$ 90 stars of each spectral type. A detection rate of 23% is measured for F stars, while G and K stars are more consistent with rates of 14% and 13% respectively (uncertainties are roughly $\pm$5%). The overall detection rate is $\sim$ 17% with 48 stars of 275 in the sample hosting a detected disk, very comparable to that found at 70 μm with Spitzer (Trilling et al. 2008), and ostensibly lower, but still consistent, with the rates measured by DUNES given their higher uncertainties (Montesinos et al. 2016; Eiroa et al. 2013).

Sibthorpe et al. further use the properties of the detected disks and the host stars to gauge the completeness of their detection rates and calculate an adjusted underlying incidence for all completeness rates above 10%. They find completeness adjusted incidence rates of 36%, 18%, 24% and 21% for the F, G, K and total samples, respectively. Thus, the F star incidence rate is found to be distinctly higher than that of the G and K stars, which are more compatible with each other. Taken in context with the A stars observed by DEBRIS (Thureau et al. 2014), the raw detection rate of the F stars is in fact more comparable to that of the A star population ($\sim$ 24%), rather than the G and K stars, suggesting that the traditional breakdown of FGK into a solar type class may not be optimal.

This is borne out by analysis of the F and K stars targeted by DEBRIS and DUNES. Sibthorpe et al. show that while DUNES and DEBRIS both target a similar fraction of early F stars, the higher number in the former survey leads to by far the higher fraction of detected disks, demonstrating a break around F4. A similar break around K4 is also suggested by the data. (The F4-K4 range was explicitly utilized by Sierchio et al. (2014).)

A declining detection rate with age is known and expected for debris disks, since they collisionally evolve over time. For example, Riviere-Marichalar et al. (2014) observed 19 members of the young β Pic moving group with Herschel and find an excess detection rate of $\sim 50\%$. Among compiled data toward several young moving groups, Moór et al. (2016) find a much lower rate of detections for K stars (20%) versus late F and G stars (56%). These data show that the trend in decreased detection rate as a function of spectral type is real, but it is more difficult to detect at later ages and in some spectral ranges than in others, i.e., the gradient of the change may be gradual but have some sharp transitions, particularly at later ages.

There remain only a few disks detected around M stars. Whether this is due to the current sensitivity limits (see Morey & Lestrade 2014, and references therein) or different progenitor properties (e.g., Gaidos 2017) is not yet resolved. The current detection rates are in the range of a few percent. The M star population is discussed at length in the review of Matthews et al. (2014b).

The multiplicity of the system may lower the rate of detected disks, but seems to have little impact on the nature of detected debris disks, which break in such cases into either circumprimary (or even circumsecondary) or circumbinary as dictated by the separation of the primary and companion (Rodriguez et al. 2015; Montet & Simon 2016).

Montesinos et al. (2016) show that an extrapolation of the fainter fractional luminosity detection rates to Solar System levels decreases significantly the predictions of the excess rate relative to the predictions from Spitzer data (Bryden et al. 2006). Montesinos et al. (2016) also verify the trend of decreasing fractional luminosity as a function of stellar age, using rotation period of the star as an age-proxy. A decline in fractional luminosity or excess is consistent with slow erosion of the disk material over time, consistent with earlier results from Spitzer (see Matthews et al. 2014b, and references therein) and as expected for the standard theory of a collisional cascade (Wyatt 2008).

2.2. Two Temperature Disks

Chen et al. (2014), in their study of 571 compiled Spitzer IRS observations of stars, found that 499 stars showed a detectable excess. They found that 66% of those disks were best fit by a two-temperature, rather than a single temperature, model based on Spitzer data alone, corroborating the results of Ballering et al. (2013). Characterization of disks is always improved by studies which can resolve the disk components, and Pawellek et al. (2014) examine systematically 34 systems in which the outer disk major axis is resolved by Herschel. They find based on their fits to the observed outer disk radius, in conjunction with SEDs, that 2/3 of the disks are better fit if a warmer component is included in the fits. This is remarkably consistent with the results of Chen et al. (2014) and both these studies are consistent with previous studies that suggest many spectral energy distributions are not well described by a single temperature dust distribution. The high number of disks that require two temperature dust distributions reinforces the idea that planets are common in debris systems, since planets are a primary, but not the only, means of excluding dust from

certain regions of a disk (i.e., Shannon et al. 2016).

While it is possible for differing size distributions and grain compositions to produce two-temperature SEDs for a single dust belt, Kennedy & Wyatt (2014) find that most two temperature SEDs likely indicate two independent dust belts, and models exist to interpret the gaps observed in disks in terms of unseen planetary bodies (e.g., Shannon et al. 2016; Rodigas et al. 2014). Chen et al. (2014) find that single temperature disks are distinct in their distribution from the two temperature populations, while the latter tends to align well in temperature with the warm and cold dust populations of the solar system, i.e., the zodiacal light and the Kuiper Belt, suggesting that in other systems as well, each component could evolve via steady state collisional cascades independently (Geiler & Krivov 2017), whereas other models suggest the transport of cometary material inward to feed warm dust belts (e.g., η Corvi, Marino et al. 2017). In contrast with earlier work (i.e., Morales et al. 2011)), the temperature of both the warm and cold components is seen to vary with stellar temperature (Kennedy & Wyatt 2014; Ballering et al. 2013), a relation that appears most acutely above stellar temperatures of 8500 K, i.e., for A stars.

Ballesteros et al. (2017) further illustrate a trend (albeit with some scatter) in the radial location of systems with only a warm dust component and stellar mass (i.e., temperature), with the dust located in a position consistent with the primordial snowline. They find no similar trend in systems with both warm and cold components, however. Collisional processing of asteroid belt analogues could provide an in-situ source of warm dust belts, at least in single dust component systems.

2.3. Exododis

Dust in the terrestrial zone, i.e., the warm dust in two-component disks, can generally be termed exozodiacal dust. In the Solar System, this dust has typical temperatures of 270 K and has as its most likely source collisions of short period comets. There is also evidence for some hot dust very close to the Sun. In other systems, both warm dust akin to the Solar Systems zodiacal light, as well as much hotter dust located closer to the host stars, has been detected. Kral et al. (2017c) provide a comprehensive review of the detections of exozodiacal dust, the common observing techniques and the potential origins of the dust observed, and we refer the reader to that detailed review and the references therein. While Kral et al. (2017c) differentiate an exozodi from a debris disk, which they define as a cold Kuiper Belt analogue, the source of both must be circumstellar material in orbit around the (usually) main sequence star, and we discuss each as a component of the debris disk.

The infrared luminosity of the zodiacal dust cloud amounts to 10^{-7} of the solar bolometric luminosity (Nesvorný et al. 2010; Roberge et al. 2012), of the same order as that of the Kuiper belt dust in the outer Solar System. Exozodis are of interest not just for insight into the underlying planetary systems, but also because their presence can significantly hinder our ability to detect planets in the habitable zone. Even Solar System levels of dust, 1000x less than the levels we can currently detect, can hinder detection of planets (Roberge et al. 2012).

To date, there have been many surveys with space-based single dishes for warm dust emission. These include IRAS, ISO, and more recently, Spitzer and WISE, as discussed above. Based on these surveys, the detection rates of warm dust was found to be quite low, in the range of 1-2% and in single dish studies, excesses at mid-IR wavelengths can be created by the Wein tail of cold dust belts (see Matthews et al. 2014b, and references

therein). The observed rates do however increase with wavelength, with the frequency increasing up to 11.8% ± 2.4% of nearby, solar-type stars at 30-34 μm, in accordance with theoretical models (Wyatt et al. 2007).

In contrast to cold dust disk components, high resolution is a critical factor in even detecting exozodi emission, even in nearby stellar systems, and significantly higher detection rates have been found through near-IR and mid-IR interferometry. Mennesson et al. (2014) and Millan-Gabet et al. (2011) present detections of mid-IR excesses from the Keck Interferometer Nuller toward 47 stars, finding detection rates above 30% for A stars with a global rate of 12%. There is a strong correlation of detection of mid-IR excesses for systems with cold dust disks around host stars earlier than F2. This suggests that there is a common physical origin for the warm disk components and Kuiper belt analogues, or that the warm dust belt is fed by the cold belt through some mechanism, in contrast to hot dust emission. Therefore, it seems that the "exozodis" measured through mid-IR interferometry are completely consistent with the warm dust components detected in concert with cold dust belts (e.g. through SEDs), albeit at much higher detection rates when these components are observed with sufficient spatial resolution.

In contrast, no mid-IR excesses have been detected around stars which host "hot dust", detected through interferometric detections in the near-IR (Kral et al. 2017a). Ertel et al. (2014) present a merged sample of 125 stars observed for near-IR excesses. Based on those data, detection rates of hot dust are seen to decline from 28% for A-type stars, to 15% for F stars, down to 10% for G and K type stars, numbers that are very similar to the most recent measured rates for cold dust components. These trends are confirmed by Nunez et al. (2017) who expand on the original CHARA survey. Ertel et al. (2014) further show that the detected rate of hot dust rises with increased stellar age, the opposite of what is expected for a collisional cascade, further suggesting that the hot dust components are not generated by a steady state process, a fact supported by the collisional lifetime arguments for dust so close to the host stars.

As for the mid-IR excesses, no obvious correlation is seen between the presence of near-IR emission and the presence of a cold Kuiper Belt analogue. Ertel et al. (2014) point out that this is a surprising result, since hot dust cannot be created in situ and therefore, it should be correlated with some outer reservoir of material from which the hot dust is drawn. As Kral et al. (2017c) describe, there are many scenarios to move material inward in a planetary system that could assist in a build up of dust in the inner parts of a planetary system. To date, however, there is no correlation seen between the presence of planets and the detection of hot dust. We note, however, that Lisse et al. (2017) find evidence for hot dust emission in ground-based spectroscopy of HR 4796A's well studied young debris disk, which has an outer cold component. Based on their data, they find that some of the excess seen in the near-IR is due to a tenuous component of 850 K with evidence of organics and silicate emission. The authors suggest that that the emission is consistent with a steady stream of dust flowing into the sublimation zone from the disintegration of rocky cometary material.

Many of the observed systems are old ($>$ 100 Myr), making the origin and high frequency of the exozodis an active area of research. The issues of timescales and depletion of dust due to collisional evolution or radiative forces are even more acute closer to the star than it is for the cold belt detected by Herschel or ALMA. In steady state, a typical amount of observed hot dust would survive for only a century; either the dust is replenished or there exists a means of keeping the dust in situ longer without dissipation (van Lieshout et al.

2014).

Modeling of a sample of nine hot exozodis found that the dust was located further from the star for higher stellar luminosities, such that the dust appears to have a consistent temperature in each system (Kirchschlager et al. 2017). The dust masses measured are in the range of a few $\times 10^{-9}$ $M_{\oplus}$. Based on the modeling, the authors also conclude that the flux is dominated by thermal emission, although they cannot exclude a fraction of the emission arising from scattered light. The compositional analysis rules out silicates since their presence is inconsistent with the absence of mid-IR excesses. A more detailed discussion of the composition of debris disk components is deferred to § 3.

2.4. Correlations with Planetary Systems

Assessing the demographics of systems with debris disks and planets is challenging. The strongest overlap in observationally favored targets for debris disks and directly imaged planets lies in young systems, since there is now evidence for higher detection rates of debris disks in such systems and sensitivities of exoplanet searches for thermal emission preclude searches in older systems where the planets are too faint for detection. The vast majority of detected planets, however, have been detected by other methods than direct imaging and lie at distances that may preclude detection of faint excess emission associated with a debris disk.

Theories may predict correlations or anticorrelations with debris disks and planets, depending primarily on the mass and orbits of the planets. For example, Raymond et al. (2012) predicts orbital instabilities in systems of giant planets will mean anticorrelation between eccentric Jupiters and debris disks, but predicts a correlation with terrestrial planets and debris disks. Large statistical samples, constructed to be as bias free as possible, are the key to establishing relations such as these. Such analyses of Spitzer (Kóspál et al. 2009; Bryden et al. 2009; Moro-Martín et al. 2007), Herschel (Moro-Martín et al. 2015) and WISE Kennedy & Wyatt (2012); Morales et al. (2012); Krivov et al. (2011); Maldonado et al. (2017) data have failed to establish statistically significant correlations of planets and debris, as have searches of planet host samples for debris characteristics (Wittenmyer & Marshall 2015). Morales et al. (2012) searched 591 planetary systems around main sequence and evolved stars for evidence of infrared excess with WISE and found an excess rate of 2.6%, but the rate dropped to 1% if only main sequence stars were considered. Kennedy & Wyatt (2012) searched for evidence of excesses more broadly and established that many potential excesses were likely spurious coincidences due to external galaxies. Smaller samples and analysis of systems in which planets are known do *suggest* however that the presence of debris correlates with the presence of (a) low mass planet(s) in the system but anticorrelates with the presence of a planet of Jupiter mass or higher (i.e., Wyatt et al. 2012; Marshall et al. 2014), consistent with the findings of Maldonado et al. (2015). This apparent contradiction stems from the nature of the samples; construction of large bias free samples is challenging (e.g., Moro-Martín et al. 2015), while the sample of stars that has been uniformly searched for debris and exoplanets is too small to yield a definitive correlation.

Wittenmyer & Marshall (2015) suggest a weak trend in brightness of debris emission as a function of planetary mass (see also Maldonado et al. 2012). In contrast, Moro-Martín et al. (2015) find no statistically significant correlation between the fraction of low or high mass planet host stars with disks or with the brightness of disks when present, compared

to stars with no evidence for planetary companions. In addition, the presence of single or multiple planets in a system also has no impact on the detection fraction or brightness of associated debris disks (Moro-Martín et al. 2015); we note however that Maldonado et al. (2012) find that the presence of planets is reflected in a lower dust luminosity in that study.

Several studies have investigated the correlations between the stars hosting debris disks and those with no evidence of circumstellar debris. The search for trends of debris disk incidence or brightness with stellar metallicity is strongly related to the presence of planetary systems. Many statistical studies have reaffirmed the established correlation of giant planets with higher stellar metallicities (e.g., Maldonado et al. 2012; Moro-Martín et al. 2015). Early studies suggested that there was no correlation of debris disks with metallicity (Beichman et al. 2006; Bryden et al. 2006). Several more recent studies have pointed out that there could be a deficit of stars with discs at very low metallicities (i.e., $-0.50 < [\mathrm{Fe/H}] < -0.20$) with respect to stars without detected discs (Montesinos et al. 2016; Maldonado et al. 2012). Maldonado et al. (2015) investigated whether any solar type (FGK) stars hosting debris show any chemical peculiarities that could relate to the planet formation process. They found no significant differences in metallicities or abundances between stars that host debris disks and those which show no evidence of debris or planetary companions. One class of stars that does appear to exhibit a relation between stellar abundance anomalies and debris disks are the λ Boo class, which show evidence that volatile elements have been deposited into the stellar atmosphere, i.e., a deficit of refractory elements. Draper et al. (2016) show that all nine such stars observed in a study with Herschel host debris disks, well above the typical detection rate for bright disks around A stars in general, albeit in a small sample. The disk components detected by Herschel are at large radii, too far away from their host stars to effectively deposit material onto the stellar surface. Draper et al. (2016) suggest the stellar chemical signatures are harbigers for other dynamical activity in such systems, related to the deposition of material in the stellar atmosphere, and the presence of a bright debris disk, such as planetary perturbations.

3. Dust properties

The appearance and SED of a debris disk is determined by its geometry and by the properties of the dust grains it contains. It is therefore possible to use observations of disks to place constraints on its dust population, in particular the grain composition and their size distribution. In this section, we first discuss the constraints on dust properties gleaned from disk-integrated observations before turning to spatially resolved observations, in which modern high-resolution capabilities lead to analyses that are much less subject to biases and degeneracies. We conclude by discussing the strengths and limitations of combining a diverse set of observations.

3.1. Spatially unresolved observations

3.1.1. Broadband SED. The broadband infrared excess of debris disks systems readily indicates the range of dust temperatures in the system. Systems with SEDs broader than a pure blackbody can be interpreted either as radially extended disks or as containing a wide range of dust grain sizes as small dust grains are warmer than blackbody grains at the same distance from the star due to their poor long wavelength emissivity. Thus, temperature-based constraints about the dust properties are affected by a severe inherent degeneracy. In cases where the emission is best described with two, well-separated temperatures, it is reasonable to assume that the circumstellar dust is distributed in two spatially separate components (see Section 2.2), but again the degeneracy between grain size and stellocentric distance remains unsolved.

The fact that small dust grains are imperfect long-wavelength emitters results in a long-wavelength tail that is steeper than the Rayleigh-Jeans law and is usually parametrized through a two-parameter opacity law, whereby the perfect blackbody emission is multiplied either by a $\lambda^{-\beta}$ term for $\lambda \geq \lambda_0$ (Backman & Paresce 1993) or by $1 - \exp(-(\lambda_0/\lambda)^{\beta})$ (Williams et al. 2004). Both λ_0 and β are related to the grain size distribution. For instance, a standard interpretation is that $\approx \lambda_0/2\pi$ represents the size of a "characteristic" dust grain in the system, i.e., an average over the entire grain size distribution weighted by mass and emissivity. With values of λ_0 generally in the 100–300 μm range (Holland et al. 2017; Sibthorpe et al. 2017), the typical grain sizes derived from such analyses range from a few to a few tens of micron. Because of the steep size distribution in debris disks, this is often interpreted as the minimum grain size in the disk.

While varying dust compositions result in different intrinsic values for the inefficiency of emission for a single grain, the effects are weak at best (Draine 2006). As a result, measurements of β primarily constrain the grain size distribution. Expected values range from $\beta \approx 1.7$–2 for interstellar medium dust to $\beta \approx 0$ for dust populations rich in millimeter-sized grains as observed in protoplanetary disks. Herschel surveys and other ground-based observations have revealed typical values of β in the 0.5–1 range (Holland et al. 2017; Sibthorpe et al. 2017), leading to a grain size distribution power law index in the 3.2–3.6 range (Ricci et al. 2015a; MacGregor et al. 2016a), in reasonable agreement with predictions from steady-state collisional cascade models (Dohnanyi 1969; Pan & Schlichting 2012; Gáspár et al. 2012). One notable exception is HD 141569, whose shallow long-wavelength SED slope suggests a size distribution index as low as 2.8 (MacGregor et al. 2016a), emphasizing the unique nature of this system.

3.1.2. Solid state emission features. More detailed information about the dust properties of a debris disk can be obtained through solid state emission features. The spectral shape of various silicate features, at wavelengths ranging from 10 to 70 μm, inform on the size, composition and degree of crystallinity of the emitting dust grains, provided they are no larger than $\approx 10\,\mu$m and heated to a minimum of 150–200 K (except for the 69 μm forsterite feature, which can be present at lower temperatures, e.g. de Vries et al. 2012). Thus, studies of the silicate mineralogy are limited to small grains in the warm and hot component of debris disks. From the Spitzer sampled analyzed by Chen et al. (2014), Mittal et al. (2015) detected silicate emission features for 120 debris disk systems. Over 80% of all objects are well fit with dust models assuming a combination of standard silicate compositions (olivine, pyroxene, forsterite and enstatite). The spectra of the remaining sources require additional species but nonetheless confirm the dominant presence of silicates in these disks. The minimum grain size inferred by Mittal et al. (2015) range from ≈ 2 to $\approx 20\,\mu$m. While these are in qualitative agreement with blow-out sizes, the dependency of the minimum grain size with stellar luminosity is significantly shallower than would be expected from simple blow-out calculations, suggesting more complicated physics. The inferred slopes of the grain size distribution span a broad range from ≈ 2 to ≈ 5, but with a typical value of 3.5–4.0, again in reasonable agreement with predictions from collisional cascade models. In addition, the study identified a broad range of crystalinity levels, from $\lesssim 1\%$ to $\approx 95\%$, illustrating the intrinsic diversity of dust properties in warm debris disks.

Many non-silicate species have spectral features in the mid-infrared. High signal-to-noise spectra, together with dedicated spectral decomposition codes (e.g., Olofsson et al. 2012; Lisse et al. 2012), can thus be used to infer their presence in debris disks. The list of species whose presence has been proposed in debris disks through such a decomposition include water ice, amorphous carbon, metal sulfides, silica, SiO and organic materials (e.g., Currie et al. 2011; Johnson et al. 2012). However, the interpretation of these decompositions is subject to several caveats. Some species (e.g., water ice, amorphous carbon, sulfides) have nearly featureless spectra which can be confused with continuum emission. Also, the unicity of solutions is uncertain given the large number of degrees of freedom in the decomposition. Finally, and perhaps most profoundly, the treatment of complex mixture (linear combination of spectra vs effective medium theory) relies on unverified assumptions about the structure of individual grains (aggregates vs collection of pure grains). The effect of this uncertainty has been illustrated in the case of η Crv disk (Lebreton et al. 2016), which thus serves as an important cautionary tale. In summary, while dust grains in debris disks are characterized by a high mass fraction of standard silicates, their detailed composition beyond these species remains uncertain.

3.2. Spatially resolved observations

3.2.1. Dust temperature and stellocentric distance. Spatially resolving a debris disk allows to solve for the ambiguity between disk radius and grain size. Specifically, it is possible to compare the measured disk (inner) radius with the "blackbody radius" based on the dust temperature derived from the SED. As expected from the fact that real dust grains are not perfect blackbody emitters, the actual size of debris disks is consistently larger than the blackbody prediction, by a factor of up to 10 times (e.g., Morales et al. 2016). These studies demonstrated that the effect is much more pronounced for debris disks surrounding lower luminosity stars, which can be partially attributed to the fact that such stars have a much

smaller blowout size. However, the ratio of the observed to predicted radii displays a scatter of more than a factor of 2 at a fixed stellar luminosity, which is not expected from a simple blowout calculation. This suggests that other effects are at play, such as object-to-object differences in dust composition, grain porosity, and/or size distribution slope. While each of these effects can be computed (e.g., Pawellek & Krivov 2015), it is virtually impossible to disentangle them based on a single disk radius estimate.

With the disk's inner radius (and radial extent) determined from an image, it is then possible to constrain more robustly the dust properties based on the SED. This is typically done by assuming either that the thermal emission is dominated by the smallest grains or that the size distribution is a power law. The resulting minimum grain sizes are again in the 1–10 μm range (Pawellek & Krivov 2015; Morales et al. 2016). Reminiscent of the analysis of unresolved observations, these studies consistently find that, while debris disks around A-type stars are characterized by a minimum grain size equal to the blow-out size, the smallest grains in disks around solar-type stars are a few times larger than the blow-out size. The dearth of grains close to the blowout size in lower luminosity stars could be an indication that debris disks around solar-type stars are subject to weaker collisions, possibly because they are less stirred.

3.2.2. Scattered light properties. The dust-related quantities that can be measured from a scattered light image include 1) the overall albedo of the disk, 2) the disk scattered light colors, 3) the scattering phase function, and 4) the degree of linear polarization. Each of these is dependent on the grain properties (composition, size, shape, ...) and wavelength. Unfortunately, the albedo is degenerate with the total dust mass for optically thin disks. More profoundly, only the Bond albedo (averaged over all scattering angles), which is not accessible from our fixed vantage point, can help constrain the dust properties. As a result, we only discuss here results based on disk colors, scattering phase function and polarization.

3.2.2.1. Disk colors. At first order, the scattered light color of a disk (relative to its parent star) is a differential albedo measurement, although this can be compounded by chromatic scattering phase function effects. Small dust grains scatter in the Rayleigh regime and disks dominated by such grains will be bluer than their parent star, whereas large grains have roughly neutral scattering colors. Furthermore, some dust compositions have markedly red albedo colors across the visible, as evidenced by the colors of Solar System minor bodies.

To date, only 10 disks have had their (optical and/or NIR) scattered light colors measured to date. As a group, they present a broad range of colors, from bluer to redder than the star. On the one hand, the AU Mic disk is consistently bluer than its parent star throughout the optical and NIR (Lomax et al. 2017, and references therein), consistent with the idea that the low-luminosity star cannot expel small dust grains through radiation pressure. However, some debris disks surrounding earlier-type stars have also been found to have blue colors in the optical and/or NIR (e.g., HD 61005; Esposito et al. 2016). Similarly, red disks (e.g., HD 107146 and β Pic; Ardila et al. 2004; Golimowski et al. 2006) are found around stars that represent a range of spectral types which partially overlaps with that of blue disk hosts, indicating that the blow-out size is not the only factor setting a disk's color.

In the few cases where disk images at $\lambda \geq 3\,\mu$m exist, the disk colors become essentially neutral, both for blue and red disks (Rodigas et al. 2012, 2015), although it remains unclear why there is such uniformity. In particular, no conclusive evidence for water ice has been obtained so far for debris disks based only on 3–3.4 μm imaging, although even $\approx$ 50%

fractional composition can be consistent with observed disk colors in at least some systems.

HR 4796 is the disk for which flux-calibrated scattered light image are available across the broader range of wavelengths, from 0.5 to 3.8 μm, enabling the most detailed dust composition analyses.The red optical-to-NIR scattered light colors have been proposed as indicative of the presence of organic compounds similar to those found on Solar System minor bodies by Debes et al. (2008a). However, similar colors can also be reproduced with porous grains primarily made of silicates, amorphous carbon and possibly water ice (Köhler et al. 2008; Rodigas et al. 2015), emphasizing the difficulties inherent to a color-based approach to constraining dust properties.

Beyond integrated colors, color gradients have been identified in several debris disks; these can have two distinct causes. One possibility is that the dust population is not uniform across the disk. The smallest grains being more sensitive to radiation pressure than larger ones, they may have different spatial distributions. Such effects are likely the root cause for lateral color asymmetries (Kalas et al. 2005; Golimowski et al. 2006). Similarly, the finding that the halos of debris disk appear consistently bluer than the star (e.g., Debes et al. 2008b; Maness et al. 2009) strongly suggest that they are dominated by submicron grains. On the other hand, color gradient can arise from wavelengths dependencies of the scattering phase function, which is expected to become increasingly isotropic towards longer wavelengths. This could for instance explain the observation that the AU Mic disk is bluest at the smallest projected separation from the star, i.e., at the smallest scattering angle (Lomax et al. 2017).

3.2.2.2. Scattering phase function. The surface brightness distribution of a debris disk is set by its volume density and the dust scattering phase function. Very small grains are expected to scatter nearly isotropically while grains much larger than the wavelength display a strong preference for forward scattering. If the disk geometry is well understood, it is therefore possible to place constraints on the dust properties.

The most common analysis tool for scattering phase functions is the Henyey-Greenstein analytical prescription that is described by a single parameter, the asymmetry parameter g, which is the intensity-averaged cosine of the scattering angle (Henyey & Greenstein 1941). Isotropic scattering corresponds to $g = 0$, while forward and back scattering are characterized by positive and negative values of g, respectively. While it is easy to implement, this formalism does not rely on a physical framework and does not have a unique interpretation in terms of dust properties. Furthermore, estimating the sign of g requires identifying which side of the disk is in front of the parent star, which is normally assumed to be the brightest as a result of preferential forward scattering, but can be ambiguous in some cases (Perrin et al. 2015; Le Bouquin et al. 2009).

Estimates of the asymmetry parameter have been obtained for over two dozen debris disks. There is considerable scatter in the resulting values, from $g = 0$ to $g = 0.85$, with no obvious trend as a function of wavelength, disk color or stellar spectral type. While it is tempting to interpret this quantity as evidence for small (isotropic) or large (forward scattering) grain size, the interpretation of the asymmetry parameter is complicated by our viewing geometry, specifically the disk inclination which sets the range of scattering angles that can be probed. Interestingly, despite a large scatter, there is a clear positive correlation between the fitted g values and the breadth of scattering angles probed by the observations. This is consistent with the idea that the scattering phase function of debris disk dust does not obey a simple Henyey-Greenstein function, but rather is generally characterized by a

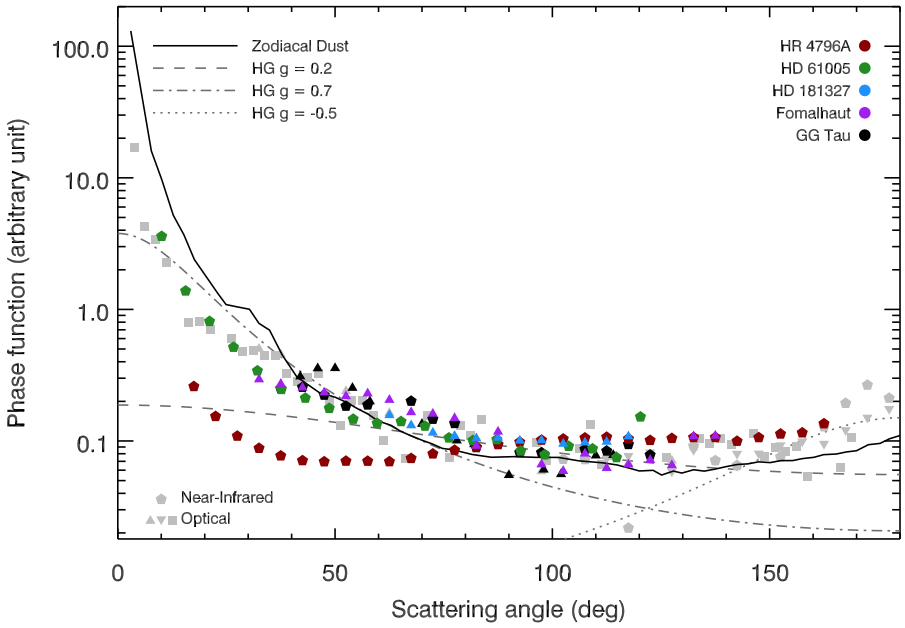

Figure 1

Observed scattering phase function for debris disks (colored symbols; Kalas et al. 2013; Stark et al. 2014; Olofsson et al. 2016; Milli et al. 2017b), the GG Tau protoplanetary ring (black symbols; McCabe et al. 2002; Krist et al. 2005), Saturn's ring dust (gray squares; Hedman & Stark 2015), cometary dust (gray triangles and squares; Hanner & Newburn 1989; Schleicher et al. 1998; Zubko et al. 2014) and zodiacal dust (black curves; Leinert et al. 1976). For consistency, we have assumed that the brighter region of each debris disk corresponds to the front side of the disk (however, see Le Bouquin et al. 2009, for the case of Fomalhaut). Near-infrared observations are shown as pentagons whereas other symbols indicate visible light observations. The gray curves display representative Henyey-Greenstein phase functions.

shallow slope around 90°, thus yielding low g value for nearly face-on disks, coupled with a strong forward scattering peak that is only sampled for disks seen close to edge-on.

A more agnostic approach consists in empirically determining the phase function in debris disks. This has only been done for 4 debris disks to date Fomalhaut, HR 4796, HD 61005 and HD 181327. These are shown in Fig 1 along with the phase function measured in Solar System dust populations and in a protoplanetary disk. None of the empirical phase functions matches a simple Henyey-Greenstein function. Furthermore, with the notable exception of the HR 4796 system, the overall shape of all phase functions are remarkably similar, with a strong forward scattering peak, a shallow slope at intermediate scattering angles and, when probed, a significant back scattering peak. The similarity of the debris disk and zodiacal dust phase functions has been pointed out by Graham et al. (2007) and Ahmic et al. (2009). Since these environments are unlikely to be characterized by the same dust populations, however, this suggest that there is a nearly universal phase function for circumstellar disks.

It is possible to predict the scattering phase function based on an assumed dust composition and grain size distribution using Mie theory, coupled with effective medium theory deal

with multi-species grains, as well as to handle grain porosity. It is also possible to numerically determine the scattering phase function of more complex grains, such as aggregates of small spheres and fractal grains (Min et al. 2016, and references therein). Indeed, scattered light analyses of Solar System dust have shown that this generic shape for the phase function can be well reproduced by large aggregates (e.g., Zubko et al. 2014; Tazaki et al. 2016). The similarity in phase function therefore suggests that debris disk dust particles share a similar structure, whereas the exact dust composition only plays a secondary role in setting the phase function. Even the unusual phase function observed in the HR 4796 system is consistent with scattering off porous aggregates with a minimum size of 20–30 μm (Milli et al. 2017b). Based on these calculations, the similarity of the various observed phase function stems from similarly porous dust grains while the minimum grain size sets the slope of the phase function around 90° scattering angle. In this context, the fact that the scattering phase function steepens with stellocentric distance in the outer halo of HD 181327 (Stark et al. 2014) is consistent with the presence of gradually smaller grains that are pushed on increasingly eccentric orbits by the stellar radiation pressure, as suggested by disk colors in other systems.

3.2.2.3. Linear polarization. Besides reducing the contrast relative to the unpolarized central star, imaging polarimetry provides another avenue to constrain the dust properties of a debris disk. Mie theory, as well as the approximate methods applicable to aggregates, yield model predictions that can be tested against observations. Not surprisingly, the most recent high-contrast instruments offer a polarimetric mode (GPI, SPHERE). While inferences about dust properties can be made in some special cases based on a polarized intensity image (e.g., Perrin et al. 2015), it is the polarizability curve that is most readily comparable to dust models. From an observational standpoint, this is a more challenging measurement, but it can prove powerful.

Polarization fractions have been measured for a half-dozen debris disks, all but one in edge-on configuration as this is the most favorable situation. In this situation, the linear polarization is consistently observed to increase with projected distance from the star out to the main belt radius, before reaching a plateau in the halo region (e.g., Graham et al. 2007; Asensio-Torres et al. 2016). The rising part of these curves indicates that the polarizability curve peaks at roughly 90° scattering angle, as is found for both model calculations and observed polarizability curves for Solar System dust (e.g., Lamy & Perrin 1986; Hadamcik et al. 2007). The net polarization fraction reaches maximum values of 20–50%, with no clear wavelength dependence in the cases where this could be probed (Tamura et al. 2006).

The observed polarizability have been reproduced with dust models with minimum grain size ranging from sub-micron to 5 μm, assuming standard compositions such as astronomical silicates and water ice. Additionally, in the case of the disk AU Mic, a porosity of up to 90% was inferred by Graham et al. (2007). The unusual polarizability curve observed for the HR 4796 ring, with a peak polarization at a scattering angle of ≈50° rather than 90°, is consistent with dust grains which behave in the Fresnel regime (Shen et al. 2009). This implies a minimum grain size of at least 5–10 μm in size (Perrin et al. 2015), in agreement with the conclusions reached from the disk color and phase function.

3.3. Global analyses

While each of the approaches discussed above provide important clues regarding the dust properties of a debris disk, they each suffer from ambiguities and potential biases. A multi-wavelength approach that combines several methodologies is required to obtain a complete picture of the dust properties. This has been attempted a number of times for debris disks; key results from these efforts are discussed below. Such analyses are based on Mie theory, as this is the only physically grounded framework that provides a self-consistent estimate of the absorption, scattering and emission cross-sections at all wavelengths. Key parameters that are generally fitted for include the minimum grain size, the index of the assumed power law grain size distribution, and the dust composition and grain porosity, although some of these are sometimes fixed to default values (the blow-out size, the canonical 3.5 size distribution index, and compact astronomical silicates, typically).

Thorough multi-wavelength analyses have been conducted for a dozen systems, with additional studies treating larger samples but with a smaller array of observations (e.g., Morales et al. 2016). Here we focus our attention on the most comprehensive studies to date. Unsurprisingly, the combined analysis of multiple datasets, especially when they cover a broad range of wavelengths, generally proves to be a stiff challenge. For instance, simultaneous fits to the SED and scattered light images often lead to large inconsistencies in terms of dust albedo and scattering phase function (e.g., Krist et al. 2010). The contradicting constraints obtained through different observations are best illustrated in the case of HD 181327, where no power law size distribution can simultaneously reproduce the disk scattered light colors, its scattering phase function and the system's SED Schneider et al. (2006). Better, yet imperfect, global fits were obtained in some systems through the inclusion of prorosity and a broader exploration of the possible dust compositions (e.g., Fitzgerald et al. 2007; Ballering et al. 2016; Olofsson et al. 2016). In these studies, the derived size distribution is broadly consistent with the collisional cascade predictions, with minimum grain sizes typically 3–5 times larger than the blow-out size, except for AU Mic in which submicron grains dominate the dust scattering and thermal emission.

While some modeling approaches retain astronomical silicates as the default dust composition, others consider a wide range of possible mixtures. Mixtures of silicates and carbon-bearing species (either amorphous carbon or organics) generally produce the best global fits (Rodigas et al. 2015; Ballering et al. 2016). While water ice is generally not a significant component to the dust mixture, Lebreton et al. (2012) found it to be an important one in the HD 181327 debris disk. Porosity of several tens of percent is also often necessary to reproduce the disk observations, although constraints are sometimes rather weak due to unsolved ambiguities (e.g., Rodigas et al. 2015). The β Pic disk is the exception, as compact grains are favored by global modeling (Ballering et al. 2016).

Despite significant successes, each of these global model is imperfect, independently of the degree of sophistication in the model being used. This suggests that one or more of the hypotheses built in the model are incorrect. This could indicate that different observations probe physically distinct dust populations. Also, departures from a single power law grain distribution, as often predicted by collisional models (Pawellek & Krivov 2015, and references therein), could explain discrepancies in constraints arising from observations in different regimes (e.g., scattered light vs submillimeter thermal emission). Finally, while it appears likely that dust grains in debris disks are relatively large aggregates, it remains computationally daunting to compute scattering, absorption and emission properties of such grains across all wavelengths from the UV to the millimeter. The use of Mie calculations

or of tractable approximations is likely to remain a common strategy for the foreseeable future despite the shortcoming of such models.

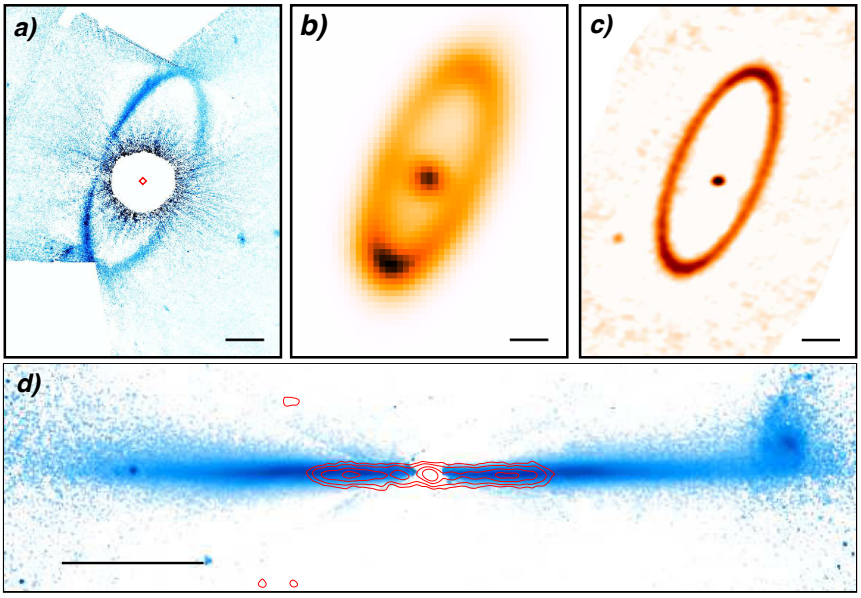

Figure 2

Top: Images of the Fomalhaut ring in HST optical scattered light (left, from Kalas et al. 2013), Herschel 70 μm (middle, from Acke et al. 2012) and ALMA 1.3 mm thermal emission (right, from MacGregor et al. 2017). The scale bars represent 50 au. *Bottom:* Overlay of the 1.3 mm ALMA thermal emission map (contours, from Daley et al. in prep) on the HST optical scattered light image of AU Mic (colorscale, from Schneider et al. 2014).

4. Outer Disk Structure

In this section, we will review the diversity and properties of spatially resolved structure in outer debris disks (exozodis and the comparison between marginally resolved outer disks and SED models are discussed in Section 2.4). Recent advances in imaging capability across the electromagnetic spectrum – for example, GPI and SPHERE at OIR wavelengths, *Herschel* at mid- to far-IR wavelengths, and ALMA at millimeter wavelengths – have revealed details of disk structure that were previously unobservable, and have begun to allow us to piece together a multiwavelength picture that connects the morphology to the underlying physics shaping the disk structure. A spectacular example of such multiwavelength imaging of the Fomalhaut debris ring is shown in Figure 2. A catalog of resolved images of circumstellar disks is maintained on the web[1].

We focus on recent observational results, particularly emphasizing disks that have been imaged at a wide range of wavelengths at at high (∼10s of au or better) angular resolution. However, it is important to note that debris disk imaging efforts stretch back across decades essentially to the moment that debris disks were discovered (Smith & Terrile 1984). *HST*, in particular, has been a consistent engine of high-resolution images of debris disks, and we include some recent results that make use of innovative data analysis techniques to draw out better contrast and reduce the inner working angle.

[1]http://circumstellardisks.org/

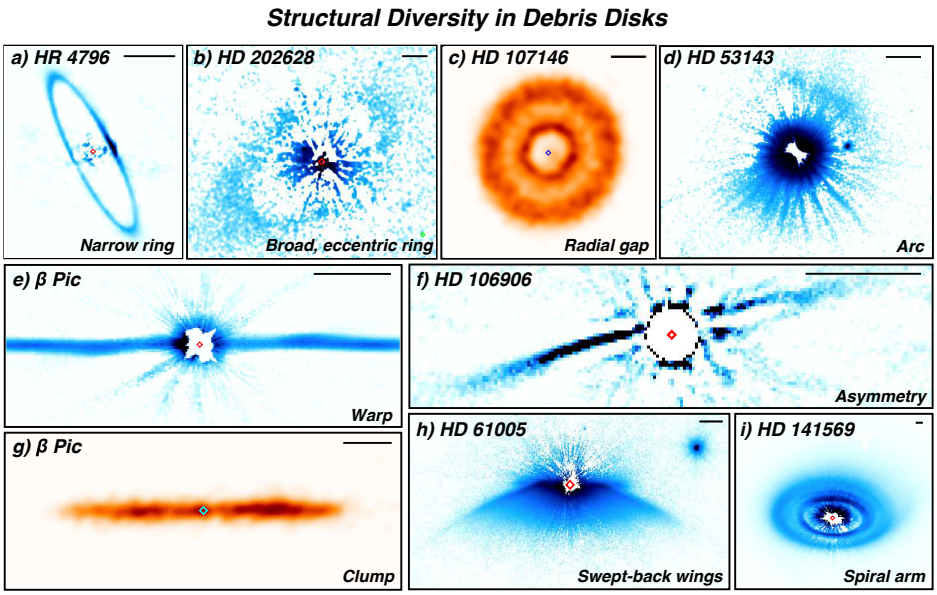

Figure 3

Mosaic of optical and NIR scattered light (blue color scale), and millimeter thermal emission (orange color scale) for eight systems illustrating the range of asymmetries observed in debris disks. The scale bars represent 50 au and diamond symbols mark the position of the central star. In some cases, smoothing and high-pass filtering has been applied to the data to better emphasize substructures. Data are from (Dent et al. 2014, panel g), (Schneider et al. 2014, panels d and h), (Apai et al. 2015, panel e), (Kalas et al. 2015, panel f), (Konishi et al. 2016, panel i), (Schneider et al. 2016, panel b), (Milli et al. 2017b, panel a) and Marino et al. (in prep., panel c).

4.1. Diversity of Resolved Structures

Here we explore the diversity of the spatially resolved structure in outer disks, divided roughly into categories of radial structure, azimuthal structure (i.e., departures from axisymmetry), and vertical structure. A summary figure illustrating examples of the different structures discussed is presented in Fig. 3. Much of this work has been enabled by advances in high-resolution imaging techniques, including large and impressive samples of *HST*-resolved disks at exquisite resolution and inner working angle thanks to improved imaging techniques like multi-roll coronography (e.g., Schneider et al. 2014, 2016) or reprocessing of archival data with improved reduction techniques like advanced PSF subtraction and artifact removal (e.g., Soummer et al. 2014). Contributions from *Herschel* and ALMA wavelengths have enabled researchers to amass high-resolution observations across the electromagnetic spectrum for the first time. We review these observations with an eye towards understanding the underlying physical mechanisms driving the diversity observed in the spatially resolved structure.

4.1.1. Radial Structure. Many debris disks are well described as a collection of rings. Some are narrow, some are broad, some systems have multiple rings or gaps within an otherwise broad ring. In this section, we explore the diversity of radial structures in debris disks and discuss connections with theoretical mechanisms describing their origin.

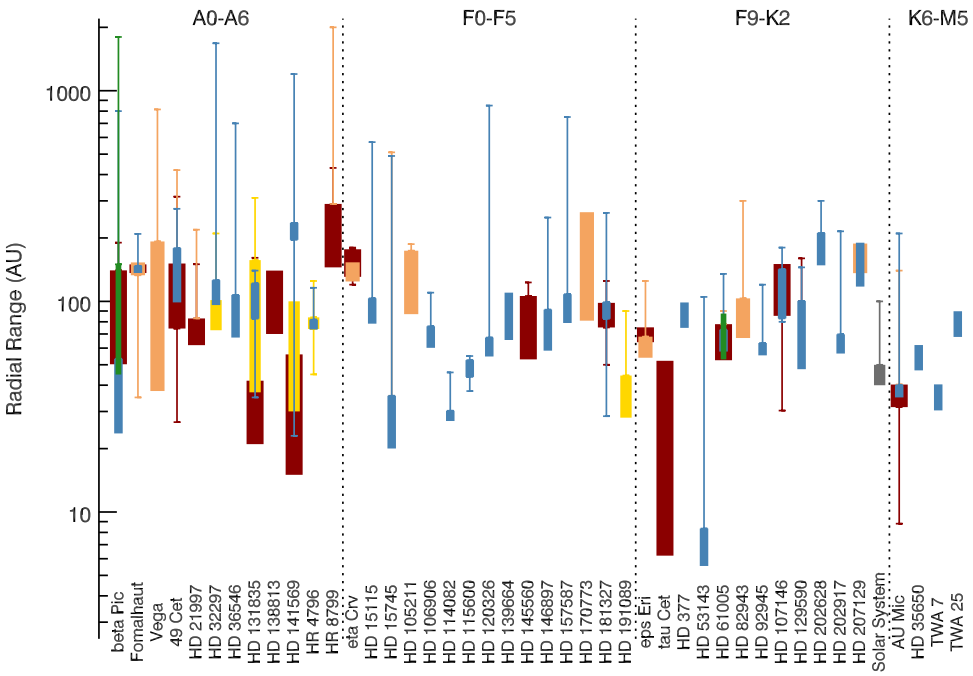

Figure 4

Radial extent of debris disks as determined in scattered light, MIR, FIR and (sub)millimeter high-resolution observations (blue, gold, orange and red bars, respectively). Green bars represent the disk structure derived from combined fits to multiple types of data. For each disk and observing methodology, the thick bar and whiskers indicate the FWHM of the inferred surface density profile and the full extent over which the disk is detected, respectively. In most cases, the latter is sensitivity-limited towards large radii, while in scattered light, the region inside the main ring is affected by severe artefacts that preclude definitive conclusions. The Solar System's Kuiper Belt is shown in gray for comparison.

Figure 4 summarizes the radial extent of all of the debris disks with well-resolved observations (i.e., the angular resolution is small compared to the disk radius) at a variety of different wavelengths. The tendency of scattered light observations to yield radially narrower structures is likely due to a selection effect (surface brightness contrast is enhanced in narrow ring) and possible methodology biases (post-processing methods to suppress contaminating starlight often partially suppress disk brightness and sharpen existing structures). Also, the need to remove the bright star from images generally leads to larger inner working angles for scattered light images, possibly explaining some of the discrepancies noted in this figure. For instance, the inner edge of the solid bar for two disks (HD 15745 and HD 53143) marks the inner working angle rather than a true inner disk edge, since the inner radius is not resolved. Similarly, our detection of the outermost region of each disk is sensitivity-limited and thus the full extent of the disks is likely underestimated. While these systems are all far dustier than our own Solar System's Edgeworth-Kuiper Belt (EKB), the radial extent is comparable: the classical EKB has an inner radius of 40 au and a width of 10 au, while the scattered belt extends hundreds of au farther in radius (Barucci et al. 2008).

There are no obvious trends in disk radius or disk width as a function of stellar spectral type. Studies of the temperature of the dust from the SED have either revealed weak

trends towards a constant temperature regardless of spectral type (e.g. Morales et al. 2011), possibly due to ice lines setting the disk location, or a slight correlation between dust temperature and spectral type suggestive of an alternative mechanism (e.g. Ballering et al. 2013; Pawellek et al. 2014), but the spatially resolved data have so far not yielded similar trends (although the sample sizes are smaller).

In general, the search for trends between disk size and stellar parameters like spectral type or age is used to distinguish between different proposed mechanisms for the dust generation that result in different patterns of radial rings. Briefly, the proposed mechanisms tend to divide into the following categories: delayed or self-stirring (e.g., Kenyon & Bromley 2008; Kennedy & Wyatt 2010), which predicts that dust is generated at larger radii with increasing time; stirring by a planet (e.g., Mustill & Wyatt 2009), in which the radius of the disk can be related to the mass, semimajor axis, and eccentricity of the stirring planet; or explanations related to ice lines or cometary sublimation (e.g., Morales et al. 2011; Jura et al. 1998). There are also explanations that tend more towards stochasticity, but rely on rare events to initiate the collisional cascade, for example a massive collision or stellar flyby (e.g., Wyatt & Dent 2002; Kenyon & Bromley 2002) and therefore are unlikely to explain the majority of the extremely commonly observed debris disk population. For a more detailed description of proposed stirring mechanisms, refer to Wyatt (2008) and references therein.

As Fig. 4 shows, the maximum radial extent of debris disks tends to be largest for the most luminous stars and smallest for the least massive, although in most cases the large outer radius is a scattered light (or IR) feature easily understood as a "halo" of small grains blown from the parent planetesimal belt by radiation pressure or a stellar wind. These extended halos are quite common around A star debris disks, with spectacular examples imaged around Vega (Su et al. 2005) and HR 8799 (Su et al. 2009). The phenomenon is not limited to A stars, however; for example, the disk around the M star AU Mic also exhibits an extended scattered light halo reaching to hundreds of au distance from the star, while the large grains traced by millimeter-wavelength thermal emission are confined within 40 au (Wilner et al. 2012, see also Fig. 2). The observed configuration in the AU Mic system was predicted by Strubbe & Chiang (2006), who proposed a model in which a "birth ring" of parent planetesimals initiate a collisional cascade, the smallest grains of which are then blown out into an extended halo. The surface brightness profile of the halo then reflects the importance of collisions relative to PR drag. This birth ring paradigm has also been observed in β Pic (Williams & Cieza 2011), with a number of other systems exhibiting extended scattered light haloes as well. A few canonical narrow ring systems, including Fomalhaut and HR 4796A (Kalas et al. 2013; Thalmann et al. 2011), also show faint extended streamers that may indicate that the phenomenon is widespread. Another interesting observation noted by Ren et al. (2017, submitted) is that at least some disks have tenuous dust haloes *inside* the parent belt, which may be populated by grains that spiral inward due to Poynting-Robertson drag.

Aside from the halo phenomenon, narrow rings (in this case meaning rings with $\Delta R/R \lesssim 0.5$) are generally quite common, with particularly spectacular examples found around the A stars Fomalhaut (e.g., Kalas et al. 2005, and see Fig. 2) and HR 4796A (e.g., Perrin et al. 2015, see also panel a of Fig. 3), as well as the F star HD 181327 (e.g., Schneider et al. 2014). There are also examples of radially broad debris disks, even when traced by large grains impervious to radiation pressure at millimeter wavelengths, including those around the A star 49 Ceti (Choquet et al. 2017; Hughes et al. 2017), the G star HD 107146 (Schneider et al. 2014; Ricci et al. 2015a, see also panel c of Fig. 3), and the M star AU

Mic (MacGregor et al. 2013; Boccaletti et al. 2015).

The question of what makes a ring narrow or broad is still a fairly open one. The broad rings around AU Mic and HD 107146 both exhibit surface brightness profiles that increase steeply with radius at millimeter wavelengths (MacGregor et al. 2013; Ricci et al. 2015a), consistent with predictions for self-stirred debris disks (Kenyon & Bromley 2002; Kennedy & Wyatt 2010), although the timescale required to assemble Pluto-size planetesimals and initiate a collisional cascade at the outer boundaries of these disks is longer than the age of the systems (Kenyon & Bromley 2008). 49 Ceti, on the other hand, exhibits a deficit of millimeter emission at small radii, with a surface density profile that generally decreases with radius beyond $\sim$100 au, extending to radii of more than 300 au. Given similar difficulties with reconciling the age of the system with the timescale for self-stirring at such large radii, it is likely that at least some parts of the disk are stirred by planets or other mechanisms (Hughes et al. 2017). Narrow rings, on the other hand, may require multiple planets shepherding the inner and outer radii of the ring (e.g., Boley et al. 2012), truncation by external perturbers (e.g., Nesvold et al. 2016) or they may be confined by mechanisms related to the interaction between gas and dust (e.g., Besla & Wu 2007; Lyra & Kuchner 2013).

Substructure in the radial dust distribution is now becoming visible as high-contrast imaging techniques improve. For example, the disk around HD 107146 contains a broad and smooth ring at optical wavelengths (Schneider et al. 2014), but is much broader and exhibits a statistically significant gap in its radial brightness distribution at millimeter wavelengths (Ricci et al. 2015a, see also panel c of Fig. 3). Similarly, the disk around HIP 73145 shows clear evidence for multiple rings (Feldt et al. 2017), as does that around HIP 67497 (Bonnefoy et al. 2017). A related phenomenon, veering into the territory of departures from axisymmetry that will be discussed in more detail below, is that of arcs and spiral arms, which have been imaged in the disks around HD141569 (e.g., Konishi et al. 2016) and HD 53143 (Schneider et al. 2014, see panel d of Fig. 3). HD 141569 may be unique in representing a truly transitional object between the protoplanetary and debris disk phases (Wyatt et al. 2015), which might explain why it is so unusual in exhibiting a clear spiral pattern (see panel i in Fig. 3), but clearly arcs and concentric rings are a relatively common phenomenon in debris disk systems. At this point the data quality is not sufficient to distinguish between gaps and multiple concentric rings in most cases, though recent high-resolution ALMA observations of the HD 107146 system are extremely suggestive of a gap-like structure that retains dust at a reduced level within the gap (see panel c of Fig. 3, Marino et al. in prep). Such a broad and shallow gap is likely to be more consistent with planet-sculpting scenarios than gas-dust interactions, and in debris systems these gaps are quite easy to open and might be sensitive to very low-mass planets (Ricci et al. 2015a).

As a final example of radial substructure, we must consider the presence of warps in debris disks. The iconic example within this category is the disk around β Pic, which exhibited a clearly warped inner disk in early scattered light imaging (Heap et al. 2000; Golimowski et al. 2006, see also panel e of Fig. 3) that pointed the way to the planet β Pic b (Lagrange et al. 2009) (discussed in more detail in Section 5). Similar structures have been observed in the disks around AU Mic (Wang et al. 2015) and HD 110058 (Kasper et al. 2015). Interestingly, modeling suggests that a single planet may produce only transient warps, and may not be able to explain all of the observed features of the β Pic system, indicating that multiple planets or other mechanisms may be necessary to sustain warped

structures (e.g., Lee & Chiang 2016, and references therein).

4.1.2. Departures from Axisymmetry. With the central star providing an essentially spherically symmetric radiation field, departures from axisymmetry are of particular interest because they require something beyond the star-disk system to break the axisymmetry. One tempting interpretation is gravitational sculpting by a planet, but other interpretations have also been proposed for various phenomena, including interactions with the ISM, gravitational perturbations from stellar flybys or companions, instabilities produced by interactions between gas and dust, and recent planetesimal collisions. Here we review several categories of non-axisymmetric structure in debris disks.

4.1.2.1. Eccentricity. A number of debris disks exhibit subtle deviations from axisymmetry in the form of eccentricity, such as Fomalhaut (Kalas et al. 2005, ; see Fig 2). These are nearly all disks with radially narrow dust rings for which a slight stellocentric offset has been observed. The detected range of eccentricities for well-resolved systems currently ranges from ∼0.06-0.2. The low end of the range is effectively set by the uncertainty of eccentricity measurements (i.e., smaller eccentricities cannot be detected using current methods), with high-resolution images of the iconic HR 4796A providing an eccentricity measurement of 0.06 ± 0.02 (Rodigas et al. 2015, and references therein), similar to the eccentricity of the HD 15115 system (Sai et al. 2015). On the high end of the range, HD 202628 has one of the highest measured eccentricities in a well-resolved system (0.18; Krist et al. 2012), and also exhibits an unusually radially broad dust distribution – making it unusual along two dimensions (see panel b of Fig 3). Other similarly high-eccentricity disks include HD 106906 (0.2; Kalas et al. 2015, see also panel f of Fig. 3) and HD 115600 (0.2; Currie et al. 2015)[2].

A detailed look at the flux distribution in an eccentric disk provides a wealth of information about the grains and their dynamics. At short wavelengths, debris disks exhibit "pericenter glow" (e.g., Wyatt et al. 1999) due to the steep r^{-2} dropoff in flux with distance from the central star: the closest point to the star (pericenter) therefore glows the brightest. At longer wavelengths, by contrast, thermal emission in an optically thin disk is proportional to the product of temperature, surface density, and opacity. The temperature decreases shallowly with distance from the star (as $r^{-0.5}$), and since the opacity at a particular wavelength should be more or less uniform throughout the disk, variations in surface density tend to dominate the brightness distribution. Since grains on eccentric orbits have the lowest velocities and therefore spend most of their time at apocenter, long-wavelength observations of eccentric debris disks tend to exhibit the opposite asymmetry from scattered light wavelengths, also called "apocenter glow" (e.g., Pan et al. 2016). Both pericenter and apocenter glow are observed in the Fomalhaut ring (see panels b and c of Fig. 2).

The variation of the apo-to-peri flux ratio as a function of wavelength can be related, in the context of steady-state models of grain populations explored by Pan et al. (2016), to properties of the grain size distribution like the power-law slope q describing the dropoff in the number of grains N as a function of their size s ($dN/dS \propto s^{-q}$) and the long-wavelength

[2]The extreme east-west asymmetry in the dusty disk around the star ζ^2 Ret has been attributed to an eccentric disk with $e \sim 0.3$, although no high-resolution images of the system have yet been obtained to confirm this interpretation (Eiroa et al. 2010).

slope of the grain absorptivity β describing the dropoff in efficiency for a grain of a particular size as a function of wavelength ($A \propto (s/\lambda)^{\beta}$ when $s > \lambda$). They apply this model to observations revealing apocenter glow in the Fomalhaut and ϵ Eri debris disks, noting that there is some ambiguity in the determination of apo and pericenter directions for ϵ Eri (e.g., Greaves et al. 2014). Recent high-resolution ALMA imaging of the Fomalhaut system have provided the first conclusive observational evidence for apocenter glow and have been used to place stringent constraints on the disk geometry and grain properties (MacGregor et al. 2017). However, detailed models of the scattered light from the HD 61005 disk perplexingly derive a density that is two times higher at pericenter than apocenter (Olofsson et al. 2016).

The underlying cause of eccentric rings in debris disks is more difficult to pinpoint. They generally break down into similar categories as the confinement mechanism in the case of narrow rings, although in this case the focus is on mechanisms that break the intrinsic symmetry of the star-disk system. The categories generally include (1) eccentric planets, including both internal and external perturbers (e.g., Boley et al. 2012; Nesvold et al. 2016; Lee & Chiang 2016); (2) interactions between dust and gas (e.g., Lyra & Kuchner 2013), although generally such ineractions require gas masses at least comparable to the dust mass, which is ruled out for several eccentric systems by existing observations; and (3) recent giant impacts (e.g., Jackson et al. 2014; Kral et al. 2015). A potential way of distinguishing between a recent collision and a more steady-state planet shepherding scenario is via the long-wavelength slope of the spectral energy distribution, since impacts are predicted to exhibit specific particle size distributions (e.g. Leinhardt & Stewart 2012).

4.1.2.2. Swept-back Wings. Another departure from axisymmetry – and one that sometimes coexists with eccentricity – is the asymmetric, swept-back features occasionally associated with dust rings in debris disks. The prototypical example is HD 61005, also poetically named "The Moth" due to the appearance of the swept-back "wings" that dominate its scattered light images (see panel h of Fig. 3). Also included in this category are HD 32297 and HD 15115[3]. Schneider et al. (2014) also note that systems like Fomalhaut and HR 4796A that exhibit low SNR evidence of faint streamers beyond a narrow dust ring may indicate that these systems are simply the most spectacular examples of a common phenomenon, perhaps due to their edge-on configuration. As a class, in addition to their large-scale asymmetries these systems feature a distinct ring component – which may be eccentric as in the case of HD 61005 (Buenzli et al. 2010) or apparently circular as in the case of HD 15115 (Mazoyer et al. 2014) – and color gradients that trace the structural asymmetries in scattered light (e.g. Debes et al. 2008b, 2009). While these systems have yet to be imaged at high resolution with ALMA, HD 15115 and HD 32297 exhibit tentative evidence of millimeter-wavelength asymmetry indicating that the large grains trace the asymmetry observed in scattered light (Maness et al. 2008; MacGregor et al. 2015a), while HD 61005 exhibits no obvious asymmetry at millimeter wavelengths, suggesting tentatively that the large grains may be confined to the parent-body ring (Ricarte et al. 2013; Olofsson et al.

[3]Schneider et al. (2014) suggest that HD 15745 should also be considered a member of the same category of objects due to its asymmetric, fan-like appearance in scattered light, although no observations have yet resolved a ring-like structure or out-of-plane substructure, unlike in the other systems. Other possible members of this category include asymmetric edge-on disks around HD 111520 (Draper et al. 2016) and HD 30447 (Soummer et al. 2014).

2016).

The most popular explanation for this morphology has so far been interactions with the ISM. An initial model for the HD 61005 system involved ram pressure stripping by cold, dense gas in the ISM (Hines et al. 2007). This system was reexamined by Maness et al. (2009), who proposed a model involving secular perturbations to dust grain orbits by a more typical warm, low-density ISM cloud. Independently, Debes et al. (2009) proposed a model involving supersonic ballistic drag from the ISM to explain the morphology of the disk around HD 32297, as well as those around HD 15115 and HD 61005. While the three models are similar in many ways, that proposed by Maness et al. (2009) requires that the relative direction of motion of the star through the ISM be perpendicular to that proposed by Hines et al. (2007) and Debes et al. (2009): rather than plowing face-on through the ISM to generate the swept-back structure of the HD 61005 disk, the Maness et al. (2009) model invokes torques from a disk plowing edge-on through the ISM to break the symmetry of the disk. Observations of the stellar and cloud velocities should eventually be able to distinguish between these two mechanisms.

Another torque-based method of breaking the symmetry, proposed by Esposito et al. (2016), involves an eccentric, inclined planet sculpting the dust in the HD 61005 system. Independently, Lee & Chiang (2016) develop a unifying model of debris disk morphology that invokes planets to explain a wide range of morphological features including needles and wings like those observed in HD 15115 and HD 61005. To provide yet another interpretation, Mazoyer et al. (2014) speculate that a recent collision like that described by Jackson et al. (2014) might plausibly explain the morphology of HD 15115. At this time, no definitive explanation for the observed structure exists, although higher-resolution imaging at long wavelengths that spatially resolves the locations of the large grains is one promising avenue of investigation, since ISM interactions generally preferentially manifest in the small grains whereas dynamical scenarios are more likely to affect the large grains.

4.1.2.3. Clumps. Clumpy structure in debris disks has long been a predicted consequence of resonant interactions between planets and debris dust (e.g., Liou & Zook 1999; Ozernoy et al. 2000). The prediction is reasoned largely on the basis of analogy with Neptune and the resonant structure it induces on Kuiper Belt objects in our Solar System; the predicted orbital period of a dusty clump is super-Keplerian, apparently orbiting with the period of the planet inducing the resonance rather than at the orbital period of the more distant KBOs themselves. Such features are most readily observed at long wavelengths that trace large dust grains, since the radiation pressure that affects the orbits of small grains can smooth over and apparently erase clumpy structure (Wyatt 2006).

While initially there appeared to be clumpy structure in low-SNR millimeter-wavelength maps of several systems, including Vega, ϵ Eridani, and HD 107146 (Holland et al. 1998; Koerner et al. 2001; Wilner et al. 2002; Greaves et al. 2005; Corder et al. 2009), follow-up observations have generally not robustly recovered the clumpy structure. There are different explanations for different sources: in the case of Vega a combination of low SNR and positioning of the features at the edge of the primary beam where noise is difficult to characterize likely led to an overestimate of the significance of the reported clumpy structures (Piétu et al. 2011; Hughes et al. 2011, 2012). In ϵ Eri, by contrast, while it is still not clear whether the features are recovered (Lestrade & Thilliez 2015; Booth et al. 2017) or not (MacGregor et al. 2015b; Chavez-Dagostino et al. 2016), it is clear that background

galaxies account for at least some of the previously reported clumpy structure, since the high proper-motion system recently passed in front of an unusually strong concentration of galaxies bright in the submillimeter (Greaves et al. 2014).

At this stage, the only system with an unambiguous departure from axisymmetry in the form of a "clump" of millimeter emission on one side is the debris disk around β Pictoris, which exhibits a relatively weak asymmetry in dust continuum emission to the SW and a stronger asymmetry in the same direction in CO emission (Li et al. 2012; Dent et al. 2014; Matrà et al. 2017b, see also panel g of Fig. 3)[4]. Unfortunately, since β Pic is viewed edge-on it is impossible to study the true azimuthal variation of the dust emission. In general, even with high-sensitivity imaging by ALMA, β Pic has so far been the primary exception to the rule that debris disks tend to be extremely azimuthally smooth at millimeter wavelengths. Since debris disks generally exhibit low surface brightness, contamination by background galaxies and random fluctuations in low SNR data are common. A robust approach to determining the role of low-SNR features is to subtract an axisymmetric model and examine the residuals (in the visibility domain, for interferometric data), but the role of background galaxies is much more difficult to determine without long-term observations that monitor changes in structure as the system moves across the sky due to proper motion and orbits the central star.

The low levels of non-axisymmetry do not rule out the presence of planets; despite the earlier predictions of resonant structure, recent sophisticated modeling of debris disk evolution that takes into account the role of collisions shows that resonant structure can be washed out by collisions even for the large grains that dominate the emission at millimeter wavelengths (Kuchner & Stark 2010; Nesvold et al. 2013). Another implication of these models is that in systems with lower dust densities where the collision rate is proportionally lower, collisions may be less efficient at washing out the signature of resonant interactions. Shannon et al. (2015) present a fast, semi-analytic method for generating images of such disks for comparison with data. Asymmetries are also expected to be more common in the terrestrial planet-forming regions, where velocities are large and destructive collisions between planetary embryos more frequent (e.g., Raymond et al. 2009). Numerical simulations of such observations have also been made in preparation for JWST/MIRI and VLT/SPHERE (e.g. Kral et al. 2015). Another potential method of distinguishing between planet and non-planet mechanisms is studying the alignment of the disk's spin axis with the parent star's rotation axis, which can be connected to planetary obliquity studies. While this field is still in its infancy, some intial strides have been made (see, e.g., Greaves et al. 2014).

4.1.3. Vertical Structure. The vertical structure of debris disks can be very difficult to measure, but can also be an interesting and important probe of the physical mechanisms shaping debris disk structure. Due to the low optical depth of debris disks, at intermediate inclinations there is a strong degeneracy between the radial and vertical structure, since a narrow ring of emission can be made to look broader either by increasing its radial width or its vertical height. The most favorable case for measuring the vertical structure is an edge-on, radially narrow disk, although even in the optimal case there is still some degeneracy between vertical structure and inclination, and in some cases at shorter wavelengths PSF subtraction can complicate the interpretation of the disk width.

[4]AU Mic also exhibits clumpiness in scattered light imaging, which is discussed in Section 6

At optical and infrared wavelengths, there have been several measurements of vertical structure in debris disks. Often these are expressed as h/r, where h is the scale height (generally Gaussian σ or HWHM of a Lorentzian or other distribution) and r is the disk radius. Among the few disks with sufficient resolution to make such a determination, there are several examples of an interesting trend in which the scale height seems to pinpoint the location of the parent planetesimal belt: these systems exhibit a projected FWHM perpendicular to the disk major axis that decreases with radius close to the star, and then switches direction to increase with radius far from the star, possibly with the outer edge of the parent planetesimal belt falling somewhere near the inflection point. For example, in the edge-on disk around AU Mic, h/r is generally observed to be in the range 0.03-0.05 (Graham et al. 2007), with two distinct regimes: within 40 au the value of h/r generally decreases with projected distance from the star, while outside $\sim$40 au it increases sharply. The transition radius corresponds to the location of the outer edge of the planetesimal ring as traced by ALMA data (MacGregor et al. 2013). Similar trends are observed for HD 32297 (Esposito et al. 2014) and HD 111520 (Draper et al. 2016), although the role of PSF subtraction in these cases is more difficult to determine than for the case of AU Mic.

The most reliable estimates of the scale height are obtained for systems in which the scattered light has been modeled within a framework that takes into account the phase function, rather than systems in which only the projected FWHM on the sky is recorded, since the projected FWHM is degenerate with the inclination of the system. Such modeling has been carried out for the disks around β Pic (Kalas & Jewitt 1995), HD 15115 (Sai et al. 2015), HD 32297 (Currie et al. 2012), HD 36546 (Currie et al. 2017), HD 115600 (Currie et al. 2015), HD 61005 (Olofsson et al. 2016), and HD 157587 (Millar-Blanchaer et al. 2016), with values ranging between 0.02 and 0.12 and a median of 0.06. An upper limit of $<$0.11 for the disk around HD 181327 is consistent with this range, and can be derived from scattered light modeling despite the nearly face-on orientation of the system (Stark et al. 2014).

The vertical structure of debris disks has often been interpreted as a measurement of dynamical excitation – indeed, the only method that can directly probe the system's dynamical state, and therefore the processes and masses of the bodies sculpting it. The large bodies stirring the collisional cascade gravitationally excite the small dust grains, increasing their eccentricity and inclination through collisions that bring the bodies into equilibrium with impact velocities comparable to the escape velocity of the largest bodies. It is therefore possible to relate the disk thickness directly to the mass of the largest bodies stirring the collisional cascade (e.g., Artymowicz 1997; Thébault & Augereau 2007; Quillen et al. 2007).

However, work by Thébault (2009) demonstrated that the vertical structure at OIR wavelengths should exhibit a substantial "natural" scale height of 0.04 ± 0.02 due to radiation pressure from the star that can excite the eccentricities and inclinations of the small grains that dominate the scattered light images, even in the absence of large bodies. Since the predicted range of scale heights is highly consistent with the observed thicknesses from scattered light observations, caution must be exercised in interpreting these scale heights as probes of the dynamical state of host debris disks. The high angular resolution and sensitivity available with the ALMA interferometer provides an opportunity to circumvent this problem by measuring scale heights at longer wavelengths, where the grains that dominate the thermal emission are large enough to be effectively impervious to the radiation pressure that produces the natural scale height at OIR wavelengths. There is even some

evidence from multiwavelength modeling that the AU Mic system should display a smaller scale height at millimeter wavelenths than at OIR wavelengths (Schüppler et al. 2015). Self-consistent modeling of the size-dependent velocity distribution in the collisional cascade by Pan & Schlichting (2012) will allow vertical scale height measurements at a particular (millimeter) wavelength to be connected with the dynamical state of the debris disk in a robust way.

5. Planet-Disk Interaction

As described in Section 2.4, there are no strong and tight correlations between the presence of planets and the presence of debris around stars. However, case studies of systems where planets and dust coexist can be extremely valuable in revealing the dynamics of planetary systems. Such studies are still in their early stages, since the ability to image planets and debris has been increasing at a rapid rate over the past decade. There are essentially two subsets of systems that have been studied using imaging techniques to understand interactions between disks and planets: systems where an RV planet (or planets) at small radii coexist with debris at large radii, and systems where both directly imaged planets and directly imaged debris dust coexist in the same system.

5.1. RV Planets with Debris Disks Much Farther Out

A number of directly imaged debris disks also coexist with RV planets in the same system at much smaller radii. In general, the relatively young stellar ages and the presence of bright dust at large radii suggest that most of these systems are stirred by planets rather than any self-stirring mechanism. While the approximate characteristics of the putative planets can be inferred via the RV method, our knowledge is typically limited to a minimum mass (or an inferred mass using the inclination derived from the aspect ratio of the debris disk, assuming that the disk and planet(s) are coplanar) and orbital period / semimajor axis.

At the time of writing, fewer than a dozen systems with RV planets also have had spatially resolved observations of their outer disks. These systems include q^1 Eri, ϵ Eri, HD 69830, HD 82943, 61 Vir, HD 38858, HD 20794, and GJ 581 (Liseau et al. 2010; Chavez-Dagostino et al. 2016; Smith et al. 2009; Kennedy et al. 2013; Marino et al. 2017; Kennedy et al. 2015; Lestrade et al. 2012). There is a catalog of stars with both debris disks and planets currently maintained by Universidad Autonoma de Madrid [5] (*GD: this could go to the "resources" box*), which should serve as a resource for updates to this list.

In most current known systems, the outer disk is only marginally resolved, and the inner edge of the debris ring is not spatially resolved at all. Its location is typically only constrained by SED models, which depend on the SED-fitted temperature (and less well-constrained size and composition) of the dust grains. *BM: made some changes above –ok? GD: yes, I think that's enough; could point to the Dust section for more detail if needed.* While there is some indication that the disks surrounding planets with larger minimum masses may have a larger radial extent (Kennedy et al. 2015), the numbers of systems sampled are far too small to draw any firm conclusions. At this stage, the most that can be said is that there is a tendency for the derived inner radius of the debris disk to be too large to be reasonably sculpted by the known planet(s) within the age of the system, implying either that there are dynamical effects not taken into account by the chaotic zone defined by Maldonado et al. (2015) or that additional planets are required to clear the region interior to the edge of the debris disk. There is also some indication that the HD 82943 debris disk may be misaligned from the planetary orbits (Kennedy et al. 2013).

[5] http://svo2.cab.inta-csic.es/vocats/debris2/

5.2. Direct Observations of Planet-Disk Interaction

Several systems have now been demonstrated to host both a directly imaged planet(ary system), often with measured orbital properties, as well as a debris disk that has been imaged at high angular resolution. Interactions between the disk and known planet(s) can now be directly observed, and the properties of the disk can, when interpreted through an appropriate theoretical framework, place dynamical constraints on planet properties like mass. Since there are currently only a handful of known systems, each one is still quite valuable. Most have been studied in great detail and provide novel constraints on planetary system properties and architectures. Here we briefly review the known systems and current efforts to understand their properties.

The first several directly imaged planetary systems also host debris disks that might plausibly be interacting with the imaged planets. This list includes HR 8799 (Marois et al. 2008), β Pictoris (Lagrange et al. 2009), and possibly Fomalhaut (Kalas et al. 2008). The latter case provides an interesting case study in planetary system imaging: before the discovery of the companion object Fomalhaut b, the eccentric debris ring around Fomalhaut seemed to require the presence of at least one eccentric planet, likely located just interior to the debris ring (e.g., Quillen 2006). With the discovery of Fomalhaut b, it seemed that the prediction had been fulfilled. However, follow-up imaging demonstrated that Fomalhaut b is actually on a highly eccentric, belt-crossing orbit that cannot be responsible for sculpting the ring (Kalas et al. 2013). Since it is now clear that Fomalhaut is not a true example of a directly-imaged planet interacting with an imaged debris ring we do not discuss it further here, but there is no doubt that Fomalhaut has more to teach us about the interaction between debris disks and their underlying planetary systems. *BM: what's the limit of the planetary body excluded based on searches vs. what's needed to explain the ring?*

The HR 8799 system is often considered to be a scaled-up Solar System analog, since it contains four giant planets orbiting between two debris belts, similar to the architecture of the outer Solar System although with larger radii and masses (e.g., Su et al. 2009). As with most directly imaged planetary systems, the masses of the planets are highly uncertain and estimated primarily based on uncalibrated theoretical models of hot- and cold-start evolution that predict the luminosity (or temperature) of the planet as a function of time. The mass derived from the observed flux therefore depends not only on the poorly understood initial conditions of the planetary system, but also on the stellar age, which can be highly uncertain, especially for isolated young A stars. Observations of the interaction between the planet(s) and debris disk(s) have the potential to help calibrate the uncertain flux-based planetary mass estimates, since the distance between the planet and the disk is a sensitive function of the mass of the planet (and its orbital properties). For example, Malhotra (1998) derive the width of a planet's "chaotic zone," which is expected to be cleared of dust, as $\Delta a \simeq 1.4 a_p (M_p/M_*)^{2/7}$, where Δa is the difference between the planet and disk semimajor axis, a_p is the semimajor axis of the planet, M_p is the mass of the planet, and M_* is the mass of the star. The width of the chaotic zone can also depend on the eccentricity of the planet (e.g., Chiang et al. 2009; Mustill & Wyatt 2012) as well as time-variable orbital parameters in multi-planet systems (e.g., Moro-Martín et al. 2010). The relationship has also been evaluated for different timescales and outcomes and extended into the brown dwarf regime (Morrison & Malhotra 2015). Planets and disks can interact in even more complex ways, and the long-term stability of the planetary system may depend on the underlying mass of the planetesimal disk producing the debris (Moore & Quillen 2013). Still, the opportunity to directly observe interactions between planets and debris is

extremely valuable due to the independent constraints on planet mass that it provides.

In the HR 8799 system, due to the large semimajor axes and orbital periods of the planets, there is still some uncertainty on their orbital parameters as well as the degree of coplanarity between the star, disk, and planetary system. Given the existing data, there are stable solutions for the planetary orbits involving a 1:2:4:8 mean-motion resonance between the four observed planets (Goździewski & Migaszewski 2014). The derived inclination of 25° in that scenario is consistent with a *Herschel*-based measurement of the disk inclination of $26^\circ \pm 3^\circ$ (Matthews et al. 2014a), although that measurement was based only on the aspect ratio of the outer disk since the inner edge was not resolved by the *Herschel* beam. On the other hand, long-term monitoring resulting in an extremely self-consistent data set favors inclinations for the planet orbits closer to 40° (Konopacky et al. 2016a), which is more consistent with the stellar inclination derived from asteroseismology (Wright et al. 2011) as well as the inclination suggested by recent ALMA imaging that clearly resolves the inner edge of the dust disk (Booth et al. 2016). The ALMA imaging also suggests that the inner radius of the dust disk may be too large for it to be plausibly truncated by HR 8799b, although the location is at least marginally consistent with the location predicted by the N-body simulations of Moro-Martín et al. (2010). Determination of the location of the inner disk edge with higher-quality interferometric data is likely to clarify its geometry and should provide the first dynamical limits on the mass of planet b.

In many ways β Pic is the best example we have of a well-understood interaction between planet and debris disk. High-resolution imaging of the debris disk has been conducted across a wide range of wavelengths (for recent examples, see e.g. Golimowski et al. 2006; Vandenbussche et al. 2010; Lagrange et al. 2012; Nielsen et al. 2014; Dent et al. 2014), so that the geometry of both large and small grains is well understood, and the planet's orbital properties are reasonably well constrained (e.g., Chauvin et al. 2012; Nielsen et al. 2014; Wang et al. 2016). After the discovery of the planet (Lagrange et al. 2009, 2010), two numerical models demonstrated that planet b was primarily or solely responsible for producing the scattered light warp (Dawson et al. 2011), and demonstrated that the orbital properties of planet b could plausibly explain not only the x-shaped morphology observed in scattered light but also the central clearing observed in thermal emission at millimeter wavelengths and potentially also the presence of a bright clump of CO emission on one side of the disk (Nesvold & Kuchner 2015a). Difficulties in placing constraints on the planet mass via these numerical simulations arise due to the uncertainty in the age of the system as well as the unknown timing of the planet's formation or scattering onto its current orbit. *BM: changed from "unknown age"*

HD 95086 hosts a system similar to that of HR 8799 in several ways: it has a two-temperature SED indicating inner and outer debris belts (Su et al. 2015) and at least one directly imaged giant planet orbiting between the belts (Rameau et al. 2013; Galicher et al. 2014). While the orbital parameters of planet b seem to be inconsistent with its ability to clear the gap inferred from the SED measurement (Rameau et al. 2016), recent ALMA imaging has placed more stringent constraints on the inner edge of the debris belt (K. Su et al., submitted). The inner edge of the debris belt is farther than the standard chaotic zone approximation would predict, leaving three possibilities: (1) the orbit of HD 95086b may be more eccentric than suggested by either the ALMA or astrometry measurements, (2) the disk and planet may not be coplanar, or (3) there may be a second planet orbiting exterior to HD 95086b but interior to the inner edge of the outer debris belt. While an additional planet is possible, its properties are fairly well restricted by the existing observations, and

it would need to be low-mass (0.2-1.5 M_{Jup}) and low-eccentricity (K. Su et al., submitted).

Even within the small sample of known stars with directly imaged disks and planets, HD 106906 stands out as unique because its perturber is external rather than internal. After the discovery of the companion object HD 106906b, which orbits at a projected separation of ∼650 au (Bailey et al. 2014), imaging of the disk revealed an extremely asymmetric dust distribution (Kalas et al. 2015; Lagrange et al. 2016; Wu et al. 2016). The ability to study planet-disk interactions in this system has provided a unique opportunity to investigate the formation mechanism of wide-separation companions, since some formation scenarios are ruled out by the timescales and geometry of the system when interpreted in the context of numerical simulations. Since external perturbers can be extremely destructive to debris dust, the timescale of evolution of the debris disk can constrain the timescale of the process that created the external perturber. Jílková & Portegies Zwart (2015) use this observation to argue for a scenario in which the current configuration resulted from planet-planet scattering from the inner disk, although their model predicts that large-amplitude osciallations should be excited through a mechanism similar to Kozai-Lidov. Nesvold et al. (2017) conduct N-body simulations demonstrating that the morphology of the disk can place constraints on the orbit of the planet, and showing that a truly exterior orbit resulting from an *in situ* formation mechanism can reproduce the observed asymmetries without vertically exciting the dust.

Finally, upcoming systems of interest in this category include two stars orbited by a brown dwarf companion located interior to a debris ring. The recently discovered companions to HD 206893 (Milli et al. 2017a) and HR 2562 (Konopacky et al. 2016b) are both directly imaged brown dwarfs orbiting interior to a debris ring inferred from SED fitting. Neither disk has yet been imaged (though both are accessible to ALMA), and it is expected that future imaging will provide useful constraints on the masses of the brown dwarf companions.

Other relevant theory papers: Internal vs. external perturber effects (Nesvold et al. 2016). Gap width with collisions – wider than predicted without taking into account the effect of collisions/eccentricity (Nesvold & Kuchner 2015b). Chaotic zone width dependence on particle eccentricity and shape of debris disk inner edges (Mustill & Wyatt 2012). Should also discuss the paper that extends the mass-semimajor axis relationship into the brown dwarf regime (was this Morrison & Malhotra (2015)?). Predicted relationship between shepherding planet's mass, semimajor axis, eccentricity, and width/radius of debris ring (Rodigas et al. 2014). Collisions damp planet-induced spatial structure (Thebault et al. 2012). Interpreting multiwavelength images to reveal planet-disk interactions (Ertel et al. 2012). Unseen planets of double-belt debris systems (Shannon et al. 2016).

BM: I've added references to Rodigas and Shannon in the two-temperature belt section of the demographics, so these models of planetary bodies for gap size are now mentioned in the body of text.

6. Variability in Debris Disks

Time domain astronomy is an exciting and expanding area of debris disk research. To date, variability studies have focused on a few intriguing sources of many ages. Below, we focus on cases of variability observed toward main sequence debris hosts. We refer the reader to a recent comprehensive review of debris disks around white dwarfs by Farihi (2016); Veras (2016).

6.1. Detections in Stellar Spectra

The observation of time variable phenomena from debris disks is not new. The variation of features in spectra were observed around β Pictoris by Beust et al. (1990); subsequent studies have confirmed ongoing detections of such transiting "falling evaporating bodies" (FEBs), or exocomets, in many A star systems (e.g., Welsh & Montgomery 2015; Eiroa et al. 2016; Montgomery & Welsh 2017, and references therin), including another member of the β Pic moving group, HD 172555 (Kiefer et al. 2014a). In edge-on systems, such bodies can be expected to cross the line of sight to the star. In a comprehensive analysis of over 1000 spectra, (Kiefer et al. 2014c) identified two different comet families within β Pictoris' disk by examining 493 individual cometary clouds. They found that one class of objects produced weak absorption features consistent with old, volatile-depleted comets in a mean motion resonance with a planet (Beust & Morbidelli 1996). A second class produced strong narrow features consistent with younger, more volatile-rich bodies on similar orbits with a very narrow range of longitude of periastron, consistent with a family of comets formed by the distruption of one or more larger bodies. The authors liken these to the Kreutz family of comets in our Solar system, a group of sun-grazing comets with periods of $\sim$ 2300 yr.

6.2. Detection in Light Curves of Circumstellar Dust

Over the past decade, variation in continuum debris disk emission over time has been detected from several sources in the form of sudden and rapid declines or increases in brightness. Disks observed to be abnormally bright in emission have been coined "extreme" debris disks. Such disks may have higher fractional dust luminosities than are typical of debris disks, i.e., $\geq 10^{-2}$ (Meng et al. 2015). They are also rare, seen in just 1% of 250 stars aged 30-130 Myr surveyed in the infrared (Balog et al. 2009). These extreme debris disks are candidates for recent major collisional events that could evolve on orbital timescales, i.e., months to decades which has stimulated a strong interest in monitoring of disks in the infrared to isolate these rare events.

Monitoring of six such disks with Spitzer has yielded evidence that four show evidence of variable emission at 3.6 and 4.5 μm (Meng et al. 2015, 2014, 2012). An additional very rapidly decaying disk around the 10 Myr debris disk host TYC 8241 2652 1 is reported by Melis et al. (2012), who attribute the decline of a factor of 30 in brightness over two years to a collisional avalanche or runaway accretion. Osten et al. (2013) propose consideration of coronal mass ejections as a mechanism for removing dust in such sources, but the timescales of its efficacy are in fact too rapid, days rather than years as observed to date.

The most well-characterized extreme debris disk is reported by Meng et al. (2014). The star, ID8, showed a sudden increase in emission followed by a year-long decay. At an age of 35 Myr, ID8 is in the right range for terrestrial planet formation scenarios. Optical observations of the star over the same period yielded no variation. In the Meng et al. (2014)

paper, the light curves at 3.6 and 4.5 μm show a significant amount of variation which the authors attribute to a new impact in the disk in 2013, in a period when the source was not observable to Spitzer. Based on the rise time of the light curve, the authors posit that the dust light curve and brightness increase records the aftermath of a large collision in the terrestrial zone between two large bodies, likely 100 - 1000 km in size. Such a collision would create an initially silica-rich vapour, from which solids would condense out with a minimum size of 100 μm based on the decay rate. Meng et al. (2015) note that the fact that the largest bodies fueling the collisional avalanche are likely mm-scale bodies producted from the impact means that a much more rapid decay phase of 100 days to 10 yr is expected compared to the underlying debris disk that evolves by a traditional collisional cascade in which the parent bodies may be 1-100 km in size (Wyatt & Dent 2002). Analysis of the light curve further places the impacted body on a period of $\sim$ 71 days, or 0.33 AU from the star.

This rapid timescale for depletion reconciles the issues of low incidence of observed extreme debris disks with the Kepler data which indicate that terrestrial planets are thought to be common around Sun-like stars (Fressin et al. 2013) and with theories that support the idea that collisions during the terrestrial planet formation phase should be common (Stewart & Leinhardt 2012). How frequently the collisions occur will then be the limiting factor in comparing the presence of a planetary system with that of an extreme debris disk.

In the near-infrared, Ertel et al. (2016) note that only one of the seven targeted sources for H-band excess in their study showed evidence for variability: HD 7788. They note, however, that since their detections are typically near their sensitivity limits, detection of variability remains challenging at these wavelengths and corroborating observations are needed. Other systems show that the H-band emission persists for years, meaning the hot dust close to the stars isn't eroding on very rapid timescales.

6.3. Detectability in Stellar Light Curves

In our traditional understanding of debris disks, the wisdom has been that while it is easier in our own solar system to observe planetesimals (comets and asteroids) that are the parent bodies that produce the dust in the debris disk, in other systems, we are restricted to observing the products of collisions: dust, and now secondary gas as well. There are now several cases in the literature of distinct, stellar light curves revealing the presence of complex circumstellar material around nearby stars that suggest the presence of larger bodies in orbit around their parent stars.

The star KIC 8462852, also known as TYC 3162-655-1 or recently dubbed "Boyajian's Star", is unique in the Kepler stellar spectral catalogue, showing complex, non-periodic behavior in its light curve with dimming events up to 20% of the stellar brightness. Boyajian et al. (2016) provide a comprehensive analysis of the light curve as well as ancillary data to provide insight into the system. Their analysis shows that the variations observed are of astrophysical origin, and they discover and rule out a companion, or stellar variation, as the source of variation in the light curve. The star shows no evidence of an IR excess, and given its distance (400 pc) we could not detect the modest amounts of dust seen around nearby stars, such as Fomalhaut (**?**). This currently restricts considerations to those plausible in a gas-poor system of planets and planetesimals. Boyajian et al. (2016) favor an interpretation of the data as a debris swarm from the breakup of one or more massive comets passing in front of the star, with an original body, or bodies, having at

least 0.3% the mass of Ceres. Ballesteros et al. (2017) instead model the system using a large ($5R_{Jup}$) ringed body shepherding a system of Trojan asteroids clustered at the L5 region, with the former producing the first, deep transit and the smaller bodies producing the period of multiple, shallow dimmings 700 days later. The authors predict that given the modeled period of 12 years, that another dimming event will occur in February 2021. Wright & Sigurdsson (2016) provides a summary of the families of ideas that have been put forth to explain the emission, which in addition to the ideas above, include dust in the system as well as artificial sources, including SETI and the construction of Dyson sphere's around the star.

In the second case, evidence of an exo-moon system in formation is seen around the Sco-Cen OB association member star 1SWASP J140747.93-394542.6 (hereafter J1407). J1407 is a 16 Myr old pre-main sequence star with a mass of 0.9 $M_{\odot}$. In 2007, a deep (dimming of more than 95%), extended eclipse of 56 days duration was observed toward this star, proposed to be caused by a large ring system in orbit around an unseen companion to the star, dubbed J1407b (Kenworthy et al. 2015; Kenworthy & Mamajek 2015; van Werkhoven et al. 2014; Mamajek et al. 2012). Kenworthy et al. (2015) conclude that the object must be bound to its host star, although its orbit have a minimum eccentricity of 0.7 and a minimum period of 10 yr. Kenworthy & Mamajek (2015) interpret a well defined gap at 0.4 AU of the 0.6 AU radius of the ring system as evidence for a $< 0.8M_{\oplus}$ satellite in formation, close to the estimate of the total mass seen in the rings.

Finally, Rappaport et al. (2017) report the detection of transits in the continuum emission of two Kepler targets. The authors report six transits over the Kepler observing period of four years toward KIC 3542116 and a single transit event toward KIC 11084727. Both stars are early F type stars and considerably fainter for spectral monitoring compared to the A stars discussed above. The search of the Kepler database was done visually, but the authors note that more such transits, showing dips at the $\geq 0.1\%$ level and lasting for hours to days, should be easily assessed in data from the upcoming TESS mission.

6.4. Directly Imaged Features

One of the enticing promises of debris disk science is the notion that substructure imaged in disks could reveal the presence of unseen planets. The β Pictoris warp, while not time variable, was one of the first obvious cases of disk structure revealing the presence of an underlying planet. Hence, searches for structure have traditionally focused on imaging of clumps or asymmetries in disks, which can then be modeled to reveal the underlying planetary architecture Wyatt (2008); Matthews et al. (2014b). In general, the orbital timescales of cold debris disk structures are too long to hope to observe rotation in real time, although warm dust on much shorter orbital periods may be imaged in future.

It is however possible to detect time variable features in debris disks images. Boccaletti et al. (2015) report the detection of five time-varying features moving outward in projection on the south east side of the AU Mic disk seen in scattered light. Using earlier epoch HST data (Schneider et al. 2014), they find that these features persist over 1-4 years and that their projected speeds in some cases exceed escape velocity, suggesting they are unbound. Boccaletti et al. (2015) further determined that the features are radially offset in each epoch, with the furthest projected features having the highest velocities. Changes in disk colour have been measured where the fast-moving features are detected, suggesting that their passage is changing the distribution of sub-micron grains at those locations (Lomax

et al. 2017). Such colour changes are in fact predicted by an avalanche origin model for the observed features.

An explanation for the features in the AU Mic disk is offered by Sezestre et al. (2017). They model the features in the AU Mic disk as arising from proper motion of the dust itself, arising from a parent body which may a planet on a Keplerian orbit, or a static case, such as the location of a recent giant collision that has generated a swarm of smaller bodies (Jackson et al. 2014). These bodies then release the dust emission in separate events, which may or may not be grouped in time. In both scenarios, the best fit models have the dust emission arising from inside the radius of AU Mic's planetesimal belt (40AU, MacGregor et al. 2013), even as close as 8 AU in the case of an orbiting planet. Sezestre et al. (2017) note that the arches seen above the disk are composed of very small grains that experience a very strong radiation pressure and particularly stellar wind forces compared to gravitational forces. While the authors note that there is a semi-periodicity in the dust release events, neither scenario offered gives a clear cadence to the events. They surmise that the release events must be tied to stellar activity.

Chiang & Fung (2017) explain the observed features as clouds of sub-micron sized dust produced in an avalanche cascade, which produces increasingly massive clouds of small dust particles as it moves through the disk. The authors posit that a disruption of a < 400 km sized body (mass $< 10^{-4}$ $M_{\oplus}$) in the AU Mic birth ring (Wilner et al. 2012) less than 3×10^4 years ago created a secondary debris ring. The avalanches are launched from the intersection of the birth and secondary rings, providing a natural cadence to the launch events, and disk rotation carries the avalanche cascade around the disk to the southeast, as observed. Because the clouds are composed of sub-micron sized grains, they experience a strong ram force, exceeding 20 times the stellar gravity. Chiang & Fung (2017) predict not only the color changes seen by Lomax et al. (2017), but also the potential to image the secondary disk if it has sufficient mass. They also note that the vertical height of the features may vary with the stellar magnetic cycle.

As discussed at the outset of this section, detections of rapid variations in brightness in debris disks, and now time variable features in disk images both could have their origin in avalanche cascades, which alter disks on timescales that can be observed and monitored to reveal the internal dynamics of debris disks. It is worth noting that both Sezestre et al. (2017) and Chiang & Fung (2017) model the emission from the AU Mic disk without requiring a perturbing planet. This highlights the fact that time variable features need not point to planet-related dynamics.

7. Gas in Debris Disks

7.1. Overview and demographics of gas-bearing debris disks

GD: I feel like some of the content of the first 2 paragraphs may be better suited for the introduction (gas has been sought - to address broad questions about its origin and evolution - to little avail at first and more often found with recent instrumental advances), keeping here only the more technical aspects (temperatures, types of emission lines, ...).

While the evolution of the dust in young planetary systems during the transition from the protoplanetary to debris stage is relatively well understood (see Wyatt 2008, and references therein), the evolution of the gas is far less constrained by observations. One of the main limitations in our understanding of gas disk dispersal is that while gas fluxes can be quite large in protoplanetary disks, the sensitivity of single-dish telescopes and interferometers has been limited due to relatively small collecting area, making gas surveys far more time intensive than dust surveys of similar-age systems. It is also challenging to detect cold gas in emission: once the inner disk has cleared, the remaining gas tends to have excitation temperatures of tens of K or less, implying that only the low-energy rotational transitions at millimeter wavelengths are sufficiently excited to be detectable, along with far-IR fine-structure forbidden lines from ground state atomic species. While surveys for gas around main sequence stars are almost as old as the study of debris disks themselves (e.g., Hobbs et al. 1985; Yamashita et al. 1993; Zuckerman et al. 1995; Coulson et al. 1998), *BM: maybe choose the oldest one as an "e.g." and leave the rest out?* the low detection rates in the early surveys were discouraging (or at least appeared to confirm that gas dissipated simultaneously with primordial dust disks). Only recently has the sensitivity of far-IR and millimeter-wave facilities become sufficient to detect gas emission from debris disks within minutes rather than hours of integration. A resurgence in interest has followed the development of large collecting area facilities like ALMA, and the study of the gas content of debris disks is now an active and rapidly developing area of study.

There are a number of questions that this line of inquiry seeks to address. One fundamental question is that of the origin of the gas: is it primordial material, indicating that gas and dust evolve on different timescales and via different mechanisms? Or is it second-generation material, like the dust in the debris disks, which might provide insight into the composition of icy bodies in distant planetary systems? We would also like to better understand the mass of the gaseous component and how it evolves, both in order to determine whether or not the gas can still dynamically influence the evolution of the dust at tens or even hundreds of Myr, but also in order to determine whether there is sufficient material to enable late-stage gas accretion by planets during the extended terrestrial planet formation stage that takes place after the dispersal of the protoplanetary disk. While it is clear that the line fluxes are low compared to those of their protoplanetary counterparts, there is still considerable uncertainty in the total mass of gas in debris disk systems due to our lack of understanding of the molecular and atomic abundances and excitation and shielding conditions within the disk.

Several heterogeneous methods have been used to probe the gas content of debris disks. They can essentially be subdivided along two dimensions: atomic vs. molecular gas, and emission vs. absorption line studies. Absorption line studies use the stellar spectrum as a backdrop against which to study the material along a single line of sight. Absorption lines are powerful probes of the atomic and molecular content of debris disks, and are responsible for detecting the largest number of distinct species in circumstellar gas, including C, O, Na,

Mg, Ca, Mn, Fe, Ni, Ti, Cr, and CO (e.g., Brandeker et al. 2004). However, there are several important caveats: the utility of this method is restricted to a relatively narrow range of inclination angles such that the line of sight from the observer to the star actually passes through the circumstellar disk and is therefore only useful for the relatively small fraction of disks seen close to edge-on. In addition, it can be difficult to distinguish circumstellar lines from interstellar lines in the same spectrum, unless the velocity of the star and the local ISM clouds along the line of sight are both well known and well separated in velocity space.

GD: It's debatable whether we should trust the results enough, but let me throw it out there as it could worth mentioning: Lisse et al. (2017) claim emission lines of atomic Si, S, Ca and Cr in HR 4796. Maybe this goes here, or in 5.2.2? Emission line studies, especially at high angular resolution, can be more straightforwardly used to study the composition and spatial distribution of material in the disk. However, since they are less sensitive to small quantities of material, they are more limited in which species they can detect. So far, the only molecular species detected in emission in debris disks is CO[6], and with the exception of imaging studies in the extremely bright and nearby β Pic system (Olofsson et al. 2001; Nilsson et al. 2012), the only atomic species that have been detected in emission in multiple disks are C and O. Complicating matters further, emission and absorption lines, at least to some extent, can probe distinct components of the disk, with emission lines dominated by the large mass reservoirs at tens to hundreds of AU from the star, while absorption lines tend to be weighted more strongly towards hot material orbiting close to the central star, often including time-variable features related to putative "falling evaporating bodies," or FEBs, in the innermost regions of the planetary system (e.g., Kiefer et al. 2014b; Miles et al. 2016). We discuss FEBs further in § 6.

Given the heterogeneity of detection methods and the non-uniformity of the sensitivity and sample selection of the various surveys conducted to date, our ability to derive robust demographic information is limited. However, the available data reveal suggestive trends and areas of opportunity in understanding the prevalence of gas-bearing debris disks. Figure 5 presents a compilation of all of the searches for – and detections of – CO, [CII], and [OI] emission from debris disk systems, subdivided by the age and spectral type of the central star. Here we limit the data to emission line studies only, since absorption line studies are more limited in their ability to provide demographic information due to the restriction on disk inclination and the difficulty of distinguishing circumstellar from interstellar features. The data are drawn from all available surveys for CO emission in debris disks, limited to systems for which the fractional infrared excess luminosity is reported to be $< 5 \times 10^{-3}$ (Yamashita et al. 1993; Zuckerman et al. 1995; Coulson et al. 1998; Greaves et al. 2000; Dent et al. 2005, 2014; Panić et al. 2010; Moór et al. 2011, 2013, 2015; Kóspál et al. 2013; Mathews et al. 2013; Matrà et al. 2015, 2017a; Hales et al. 2014; Hardy et al. 2015; Lieman-

[6]While there have been reports of other gas-phase molecular species in debris disks, they have so far not held up to further scrutiny. A gas-phase SiO feature was identified in the spectrum of HD 172555 by Lisse et al. (2009), though absorption spectroscopy and additional analysis by Wilson et al. (2016) indicate that the feature likely originates from solid-state rather than gas-phase material. Similarly, a claimed detection of H_3^+ in the disk around HD 141569 was later superseded by a more stringent upper limit (Goto et al. 2005), as were a claimed detections of H_2 in the β Pic (Chen et al. 2007) and 49 Cet (Carmona et al. 2008) disks. There is also a likely detection of fluorescent H_2 emission from AU Mic (France et al. 2007), although its origin has not been definitively localized to the disk.

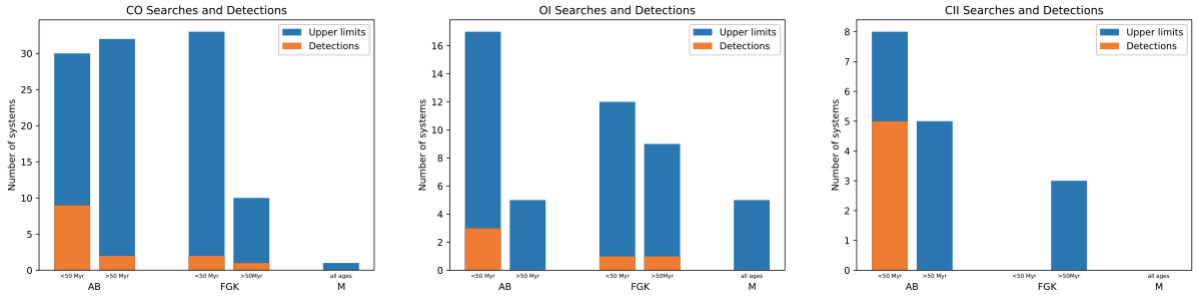

Figure 5

Histogram of all searches for (blue) and detections of (orange) gas emission from debris disks in millimeter-wavelength CO (left), [OI] 63 μm (center), and [CII] 157 μm (right), divided into bins on the basis of stellar age and spectral type. While the non-uniformity of the sensitivity and sample selection limit our ability to draw robust conclusions about the true incidence of gas-bearing systems, the available data provide suggestive evidence for greater incidence around younger stars and more massive stars, and indicate a need for more data on M star systems.

Sifry et al. 2016; Marino et al. 2016; Greaves et al. 2016; Hughes et al. 2017; Péricaud et al. 2017). *GD: This long list of reference could go in the "supplementary table" if we can find a way to present all of this that makes sense.*

Several commonalities emerge from this figure. For all three species, the highest detection rate occurs among young (<50 Myr) intermediate-mass stars. Similarly, not only are the detection rates higher for young AB stars than older AB stars, but at least for the two species with sufficient numbers to examine the question, in both cases the AB star detection rates are higher than the FGK star detection rates. The trend of higher gas detection rates around young intermediate mass stars was previously noted by Lieman-Sifry et al. (2016), who surveyed 23 debris disk host stars in the 10 Myr-old Sco-Cen region and detected strong CO emission from three of seven intermediate-mass stars but none of the 16 FGK stars.

Interestingly, the FGK star detection rates appear to be flatter with age than those of the AB stars, although of course subject to limitations in the non-uniformity of the sample. It is difficult to draw any conclusions about the prevalence of gas in M star debris disks, since only one disk has been surveyed in CO and none in CII; while a few have been surveyed in OI, the number is so small that even if the prevalence of gas-bearing debris disks were similar to those around more massive stars, we would not expect to have detected any.

The highest fractional gas detection rate occurs for young A stars surveyed in the CII line. While this might be a sample selection effect (if, for example, CII searches were targeted preferentially at previously known gas-bearing debris disks), at least one of the five detections (η Tel) occurs in a system with no previous CO detection despite a sensitive search for CO(3-2) emission (Moór et al. 2015). Interestingly, the CII non-detections in this young A star category all come from disks with at least one other gas species detection: HIP 73145 and HD 21997 (detected in CO but not OI), and HD 172555 (detected in OI but not CO). Detailed analysis of detections and nondetections within each system have the potential to reveal information about the composition of the gas; for example, the nondetection of OI in the 49 Ceti system despite abundant CO and CII emission likely points to an anomalously high C/O ratio (Roberge et al. 2013).

In addition to the detection rates, it is also instructive to examine the detected fluxes in comparison with the range of upper limits. Inspired by Fig. 4 from Wyatt et al. (2015), Fig. 6 plots the flux of each gas detection or upper limit, normalized to a distance of 100 pc,

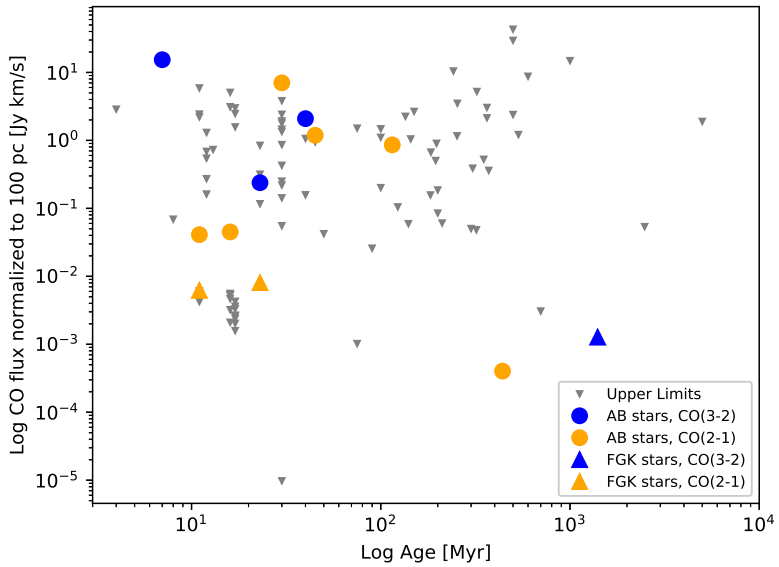

Figure 6

Flux of CO upper limits (gray triangles) and detections (colored symbols), normalized to a distance of 100 pc, as a function of stellar age in Myr. The stellar spectral type of each detection is indicated by the symbol (circles for AB stars and triangles for FGK stars), while the rotational transition is indicated by the color (blue for CO(3-2) and orange for CO(2-1)).

as a function of stellar age, with symbols dividing the detections by stellar spectral type and colors by the rotational transition of the detected species. For systems where more than one CO transition was detected, we plot only the transition with the highest-SNR detection.

The difference in normalized flux between the brightest and faintest CO detection spans nearly 4 orders of magnitude, indicating that the range of CO flux is intrinsically broad. Between those extremes, there is no obvious concentration at any particular flux level, although there is a gap of nearly two orders of magnitude between the faintest CO detection around an AB star (Fomalhaut; see Matrà et al. 2017a) and the next-faintest AB star CO disk. Since Fomalhaut is one of only a few stars that has been searched for CO to such exquisite sensitivity, it is possible (perhaps likely) that many other systems might harbor comparably faint CO disks.

The three FGK star detections are all clustered within a relatively narrow range of values between 10^{-3} and 10^{-2} Jy km/s, which is about two orders of magnitude lower than the median value for the AB star detections. This gap in flux suggests that the CO disks around FGK stars may be intrinsically fainter on average than those around AB stars. The difference is unlikely to be due to stellar temperature alone, since the gap is far larger than the expected factor of 2-3 difference in brightness due to the difference in temperature between a typical AB star and a typical FGK star given a CO disk of comparable mass.

While these broad demographic trends are suggestive, important recent insights into the nature and origin of the gaseous component of debris disks have come from detailed

observations and modeling of individual objects. In the sections below, we discuss the current state of our understanding of the gas composition, its total mass and corresponding implications for its lifetime, and the spatial distribution of material. We conclude with a summary of the current state of understanding of the origin of the gaseous component in gas-bearing debris disks.

7.2. Composition of Atomic Gas

Since CO is the only gas-phase molecular species that has been definitively detected in multiple debris disks so far, most of our insight into the composition of the gas comes from atomic lines, primarily observed through absorption rather than emission spectroscopy. Multiple-line data and modeling exist for only a handful of systems; the richest data set currently exists for β Pictoris, followed closely by HD 141569 and 49 Cet. Here we review the current understanding of the composition of gas in these systems, with notes on some other systems of interest that provide information about either unique aspects of composition or the variation of composition between systems.

7.2.1. β Pictoris. The debris disk around the nearby A star β Pic presents the richest case study in the composition of debris disk material. The unusual presence of Ca and Na absorption in the stellar spectrum was first noted by Slettebak (1975), predating the discovery of debris disks by almost a decade. The absorption spectrum of β Pic includes both a "stable" component at the velocity of the star, as well as a redshifted time-variable component that has been linked to the presence of FEBs in the innermost regions of the disk. Brandeker et al. (2004) detected and spatially resolved the disk in resonantly scattered emission from 88 different atomic lines and demonstrated that the stable Na I absorption component originates from the extended disk and suggested that the other stable spectral components probably did as well. Efforts to characterize the disk composition have therefore focused on the stable disk component rather than the time-variable FEB features.

Much of the current understanding of the disk composition hinges on the abundance of C and the C/O ratio, partly due to the generally high cosmic abundance of C and its corresponding importance to the chemistry and dynamics of gas in debris disks, but also because the C/O ratio in particular has been demonstrated to affect the outcome of the planet formation process (e.g., Kuchner & Seager 2005). An analysis of absorption spectroscopy of C+ and OI by Roberge et al. (2006) demonstrated that C was extremely overabundant, by more than an order of magnitude, relative to every other measured element, a conclusion later confirmed by *Herschel* observations of CII emission (Cataldi et al. 2014). When interpreted in the context of theoretical work by Fernández et al. (2006), the enhanced C abundance (by $> 10\times$ Solar) explains the previously perplexing persistence of the atomic gas disk, which should be subject to such strong radiation pressure that it should be rapidly cleared from the system. The high ionization fraction of the abundant C gas causes coupling into a fluid due to Coulomb collisions, which can stabilize the gas by self-braking. In addition to the extreme overabundance of C, Roberge et al. (2006) also derived abundances for a number of different elements showing that lithophile (e.g., Mg, Al) elements have roughly solar abundance relative to each other, as do siderophile elements (e.g., Fe, Ni), though lithophile elements are slightly underbundant relative to siderophiles.

The other interesting feature uncovered by absorption spectroscopy was a C/O ratio that exceeds the solar value by a factor of 18. Detection of [OI] 63 μm emission by Brandeker

et al. (2016), however, implied a lower C/O ratio due to a higher inferred O column density. Untangling the different values implied by the emission and absorption spectroscopy requires the spatial distribution of the material, since modeling suggests that a clumpy spatial distribution is required to achieve O densities high enough to excite the observed emission. Another possibility is that some of the O is coming from the photodissociation of H_2O, which would suggest an H_2O/CO ratio of ~ 1.5 (Kral et al. 2016). The β Pic gas disk shows strong deviations from axisymmetry, with the atomic emission lines imaged by Brandeker et al. (2004) brighter along the NE limb of the disk while the CO and CI appear to be brighter in the SW (Dent et al. 2014; Cataldi et al. 2014). These opposite asymmetries may be explained by a region of enhanced electron density to the SW, which would excite [OI] emission but remove Na and Fe since they would experience more frequent recombination and therefore spend more time in their neutral form that is more susceptible to the effects of radiation pressure.

Despite several sensitive searches, a stable H component has never been detected, although the variable component exhibits Ly α emission (Wilson et al. 2017). The limits are so sensitive that they rule out a Solar abundance relative to Fe, and therefore imply that the gas disk is unlikely to be a disk remnant or gas expelled by the star. The measured column density in the infalling component is also too high to originate from a CI type chondrite meteorite, and therefore Wilson et al. (2017) suggest that the origin of the gas might lie in the dissociation of water from evaporating comets.

In general, it is clear from the atomic line studies both that C and O are overabundant relative to refractory elements, and that the C/O ratio exceeds that of the star. The updated O column density from Brandeker et al. (2016) weakens the Roberge et al. (2006) argument for a vaporized parent body somewhat, and modeling by Xie et al. (2013) presents a more detailed theoretical model favoring the preferential removal scenario even in the absence of increased O.

7.2.2. Atomic species in other systems. The inventory of stable gas components observed in absorption along the line of sight to 49 Ceti includes atomic lines of Mg, Fe, and Mn (Malamut et al. 2014) as well as C, O, Cl, S, Si, Al, and Fe (Roberge et al. 2014). This inventory includes lines from excited fine-structure energy levels, which are not seen in the local ISM and must therefore be excited in the circumstellar disk. A preliminary analysis of abundances in the circumstellar gas component of the 49 Ceti system indicates that this system, like β Pictoris, exhibits an extreme C overabundance relative to Fe (Roberge et al. 2014). The 49 Ceti system also appears to require an enhanced C/O ratio several times that of the Solar System, which is more extreme than the C/O ratio derived for β Pic.

The line inventory by Roberge et al. (2014) also includes a non-detection of CO in absorption, which is surprising given the strong CO emission observed from the spatially extended circumstellar disk orbiting nearly edge-on to the line of sight at an inclination of $79.4^\circ \pm 0.4^\circ$ (Dent et al. 2005; Hughes et al. 2008, 2017). The lack of CO absorption constrains the scale height of the molecular gas disk to be smaller than that of the atomic gas disk and restricts the flaring angle to $< 10^\circ$ (*GD: we should convert this to an h/r ratio to make for an easier comparison with the vertical structure subsection above*). A vertically thin configuration for the molecular gas is consistent with the analysis by Hughes et al. (2017) demonstrating that the vertical structure of the gas disk is spatially unresolved by the 0.4" (24 au at 61 pc) angular resolution of the ALMA observations, which is inconsistent with the expected scale height for a gas with primordial composition (mean molecular weight

~2.37). The compact vertical extent of the molecular component of the disk therefore provides circumstantial support for a high mean molecular weight gas. It is not yet clear whether the differing scale heights of the atomic (*GD: I missed where this has been discussed*) and molecular gas distribution arise from an atomic skin surrounding a molecular core, or whether the atomic gas preferentially arises from a parent body distribution with a large range of inclinations; however imaging of the recently detected CI emission from the system (Higuchi et al. 2017) is likely to provide some clues.

Despite its relatively modest inclination of $60^\circ \pm 3^\circ$ (Flaherty et al. 2016), the disk around HD 141569 also exhibits stable absorption features in MgII, FeII, and MnII that are likely to arise from circumstellar rather than interstellar material (Malamut et al. 2014), as well as atomic emission in OI and CII (Thi et al. 2014) and molecular CO emission (Flaherty et al. 2016; White et al. 2016). Like 49 Ceti, modeling of the observed emission lines prefers a disk that is flatter than hydrostatic equilibrium for a disk with primordial abundances (Thi et al. 2014). Mirroring β Pic, the small grid of models explored was unable to reproduce the observed [OI] 63 μm line flux, although in this case the models overpredicted rather than underpredicted the flux.

Information about the composition of gas in other disks is far more scant, and in most cases sophisticated modeling to integrate information from different observing methods in a given system has yet to be attempted, which presents an opportunity to integrate theoretical understanding of the phenomenon of gas-bearing debris disks. For example, HD 32297 exhibits a stable line-of-sight absorption component in Na I that is five times as strong as that of β Pic (Redfield 2007), along with CO and CII emission indicating substantial molecular and atomic gas reservoirs (Donaldson et al. 2013; Greaves et al. 2016). The disk around HD 172555 exhibits a stable Ca II absorption feature, but only variable Na I D lines, indicating a Na I / Ca II ratio that deviates significantly from ISM ratios in the same sense as the anomalously low Na I / Ca II ratio measured for the β Pic disk (Kiefer et al. 2014b). It also exhibits OI emission (Riviere-Marichalar et al. 2012).

In general, atomic line studies paint a picture of an atomic disk component that deviates significantly from the primordial interstellar medium, with evidence of both enhanced C abundance and likely high C/O ratios in multiple systems.

7.3. Molecular Gas: Quantity, Spatial Distribution, and Composition

While there is good evidence of anomalous abundances and high volatile content in the atomic component of gas in debris disks, the relationship between the atomic and molecular components is not yet well understood. Constraints on the composition of the molecular gas are scarce and depend largely on the unknown abundance of H_2 in the disk. Complicating matters, there is also mounting evidence that the presence of gas in debris disks is not a monolithic phenomenon, but rather that there are likely to be at least two classes of gas-bearing debris disks: some with primordial origin and some with secondary origin, possibly with a continuum in between.

7.3.1. Spatial Distribution. The spatial distribution of molecular gas in debris disks is one of a number of potential indicators of the origin and evolutionary status of the disk. Generally speaking, there are three interesting properties of the spatial distribution of the dust that can provide clues to its origin: 1. the degree of axisymmetry, since non-axisymmetric indications of second-generation origin given that they should shear out within a dynamical

timescale; 2. the spatial distribution of dust versus gas, since if the gas origins are secondary, we expect them to match the distribution of debris dust; and 3. the spatial distribution of gas in debris disks versus protoplanetary disks, since the latter host gas density profiles that decrease gradually over a wide range of radii and debris gas disks that do the same may indictate a common origin that rings and arcs do not. *GD: could use a reference to Williams & Cieza 2011 ARAA for discussion of protoplanetary disk gas/dust extents.*

Symmetric systems in CO emission (HD 141569, HD 110058, HD 131835, HD 138813, HD 32297, 49 Ceti, HD 21997, HD 181327, HD 146897, HD156623) are so far more common than obviously asymmetric systems (β Pic, Fomalhaut), although the current observations limit our ability to distinguish deviations from axisymmetry in most cases to within several tens of percent, and the issue of optical depth also complicates our ability to distinguish subtle contrast within the density distribution. It is also worth noting that a few systems, while dominated by a symmetric CO distribution, exhibit minor asymmetries with no obvious explanation (HD 141569, 49 Cet; White et al. 2016; Hughes et al. 2017). There are a couple of cases for which the angular resolution or SNR is insufficient to distinguish any degree of axisymmetry (η Crv, HD 23642). It is perhaps notable that the oldest star with detected CO emission – Fomalhaut, at an age of 440 Myr – is also the system with the most asymmetric gas distribution. The asymmetric debris observed in β Pic is consistent with theoretical predictions for long-lived asymmetry at the sites of recent impacts between planetary embryos (Jackson et al. 2014).

As for the comparison of the spatial distribution between dust and gas, several different configurations emerge. The asymmetric CO disks around β Pic and Fomalhaut both exhibit gas that traces closely the location of dust continuum emission in the system, enhancing the evidence for a common second-generation origin. The edge-on β Pic disk exhibits a weak asymmetry in dust continuum emission between the northeast and southwest disk limbs that is exaggerated in CO (Dent et al. 2014), while the location of the CO gas in Fomalhaut's eccentric dust ring corresponds at least approximately with the location of pericenter (Matrà et al. 2017a), although the dust emission otherwise demonstrates no deviations from axisymmetry (MacGregor et al. 2017). Among the systems with generally axisymmetric gas disks, most that have been imaged at high resolution seem to exhibit marked differences between the radial extent of the gas and dust emission (HD 21997, HD 141569, 49 Ceti, Kóspál et al. 2013; Moór et al. 2013; White et al. 2016; Hughes et al. 2017), although at least one (the only F star) exhibits cospatial gas and dust (HD 181327 Marino et al. 2016). Due to the coarse angular resolution of the survey by Lieman-Sifry et al. (2016), it is not yet clear how the extent of the gas and dust disks (i.e., HD 110058, HD 131835, HD 138813, HD 146897, HD 156623) in the sample compare. The overall picture that emerges is therefore one in which asymmetric gas disks are observed to closely trace the parent dust distributions, as expected for a common second-generation origin, while the relationship between gas and dust in the systems with symmetric (and, typically, extended) gas disks is more ambiguous.

Finally, a comparison between the gas surface density profile observed in symmetric debris disks and that typical of protoplanetary disks is theoretically possible, although in practice is complicated by our lack of understanding of the excitation conditions and general lack of multiple tracers of gas in debris disks. Observations of the 49 Ceti disk at 0.4" resolution with ALMA yield surprising evidence for a CO surface density distribution that increases with radius, which is the opposite of protoplanetary disk surface density profiles (Hughes et al. 2017). Our ability to measure the surface density profile, however, hinges on

the unknown optical depth of the disk; while the CO(3-2)/CO(2-1) line ratio is consistent with marginally optically thin gas, a scenario in which the H_2 abundance is low leads to higher optical depths that might still be consistent with the line ratio, and might obscure the underlying surface density trend. A similar analysis of the HD 21997 gas disk yielded poor constraints on the variation of CO intensity with distance from the central star, due to low angular resolution (Kóspál et al. 2013). SMA observations of the CO emission from the HD 141569 disk provide a similarly broad posterior distribution, although a surface density that decreases with radius is favored (Flaherty et al. 2016).

7.3.2. Quantity, and Therefore Lifetime, of the Gas. The path from CO flux to CO mass is not been straightforward. Since observations of molecular gas are time consuming, discovery surveys and initial reconnaissance have typically been limited to single lines in the CO rotational ladder, with follow-up in multiple lines and isotopologues only recently gathered for some systems. The excitation and optical depth of the CO gas is therefore highly uncertain for most systems.

Knowledge of the CO mass and excitation affects our understanding of the gaseous component of debris disks in a number of ways. For example, dynamical interactions between gas and dust can shape the morphology of debris disks and cause features like narrow eccentric rings that are generally attributed to the presence of planets (e.g., Lyra & Kuchner 2013), although only when the gas masses are sufficiently large, in the range of $M_{gas}/M_{dust} \gtrsim 1$ (e.g., Takeuchi & Artymowicz 2001; Besla & Wu 2007).

One major question is that of the lifetime of the gas, which can generally be estimated by dividing the mass of the gas by the rate at which it is photodissociated. The lifetime of the gas is an important indicator of primordial vs. second-generation status, since a lifetime shorter than the age of the star would be a clear sign that the material must not be primordial. This knowledge is also important in determining the rate at which CO must be replenished to retain a second-generation gas disk for a significant length of time, which can aid in distinguishing which methods of gas production are reasonably consistent with the required rates. The main problem is that the rate at which CO is photodissociated depends not only on the production rate of the relevant photons by the star, but also on shielding: both self-shielding by CO if found in sufficient quantities, and shielding by H_2, which depends on the generally unknown CO/H_2 abundance (e.g., Visser et al. 2009).

Several lines of evidence point to a low H_2 abundance in debris disk systems. One is the typically low excitation temperatures indicated by multi-transition line measurements (e.g. Kóspál et al. 2013; Dent et al. 2014). These low excitation temperatures appear common, though not universal (49 Ceti's disk-averaged excitation temperature is 44 K, which is not clearly subthermal). Another is the previously mentioned lack of CO absorption along the line of sight to 49 Ceti, combined with the spatially unresolved vertical structure of its highly inclined CO disk, which indicates a molecular gas scale height smaller than that predicted for a primarily H_2 disk and suggests that the mean molecular weight is substantially larger than an ISM-based value (Roberge et al. 2013; Hughes et al. 2017). Taking the excitation temperature measurement further with the help of a non-LTE line analysis, Matrà et al. (2017b) demonstrate that the line ratios in the β Pic system are incompatible with a primordial CO/H_2 ratio, and derive a $CO+CO_2$ ice abundance of at most $\sim$6% in the molecular gas disk.

Overall, the gas masses derived for these disks are low, of order a Pluto(?) mass or less, and the lifetimes are short, typically kyr or less.

7.4. Origin

Modeling efforts to understand individual disks have recently begun to converge into a more comprehensive theory of the origin and nature of gas in debris disks.

There are a number of different proposed second-generation mechanisms for producing the observed gaseous component of debris disks. These generally include photodesorption (Grigorieva et al. 2007), collisional vaporization of icy dust grains (Czechowski & Mann 2007), either at the site of a resonant point with an unseen planet or as the result of a recent major collision between planetary embryos (Jackson et al. 2014), collisional desorption from comets (Zuckerman & Song 2012), or sublimation of comets (Beust et al. 1990). While it is not possible to completely disambiguate these various scenarios based on existing observations, there are hints that particular scenarios may be favored for different systems. For example, the highly asymmetric nature of the gas around β Pic and Fomalhaut suggests either a recent collision or series of collisions due to orbital configurations that enhance the likelihood of collisions in a certain area of the disk (Dent et al. 2014; Matrà et al. 2017a). There are some systems for which the cometary sublimation rate required to sustain the observed gas mass is uncomfortably large (e.g. HD 21997, Kóspál et al. 2013). But overall, these are generally viable scenarios for liberating dust from its solid form on the surfaces of dust grains or the interiors of comets and sustaining a rate comparable to that needed to produce the observed CO line fluxes.

An important recent attempt at unifying observations of CO, C, and O, which together comprise the dominant mass constituents of debris disks (with most of the C and O likely generated from photodissociation of CO), comes from Kral et al. (2017b). They use a semi-analytical model that assumes an input CO rate tied to the fractional excess luminosity of the disk, and then allow the gas to evolve by photodissociation and viscous spreading. Their line flux predictions are consistent with most of the detections of C, O, and CO lines in debris disks. Systems with CO fluxes that exceed the predicted values by more than two orders of magnitude are interpreted as likely long-lived primordial systems (HD 21997, HD 131835, HD 138813). Several CO nondetections in gas-bearing systems (η Tel, HD 172555) are explained by this model as due to temperatures too high to retain volatiles or high stellar luminosity that shortens the CO lifetime. The perplexing presence of C lines around intermediate-mass stars that should experience high levels of radiation pressure is explained for the first time by appealing to efficient shielding from the low levels of CO present in the disk.

According to the Kral et al. (2017b) model, most gas-bearing debris disks can be comfortably interpreted within a second-generation scenario. However, this model does not explain the much higher prevalence of gas-bearing disks around intermediate-mass stars relative to solar mass stars, and in fact predicts CO detections around 5 systems that have been surveyed with ALMA and resulted in non-detections (Lieman-Sifry et al. 2016; Olofsson et al. 2016). However, the upper limit exceeds the predicted flux by a factor of 2, indicating that more sensitive observations are necessary to determine whether or not the model can explain the lack of detections of CO in FGK star disks. The reliance on fractional excess luminosity to predict the CO flux is also somewhat at odds with the observational trend that millimeter continuum flux does not appear to be strongly correlated with the presence of CO at 10 Myr (Lieman-Sifry et al. 2016).

Overall, some gas-bearing debris disks are clearly primordial, like HD 21997, and some are clearly second-generation, like β Pic and Fomalhaut. For other systems, while most can be plausibly explained by a second-generation scenario (Kral et al. 2017b), there are

also some at younger ages and higher CO fluxes that might plausibly include a primordial component as well.

It seems clear that an unexplored dimension of the gaseous component of debris disks is their chemistry. Molecular line surveys therefore have the potential both to disambiguate the origin of individual disks, and also to potentially reveal the chemistry of exocomets. Now that more edge-on gas-bearing debris disks have been identified, there are also opportunities for expanding the available data on the atomic component through a combination of absorption and emission line studies. Since a large part of the uncertainty in the composition and origin of the disk comes from uncertainty in the molecular hydrogen abundance, it would seem fruitful to follow up on the detection of fluorescent H_2 emission from AU Mic in other nearby systems. And finally, filling out the sample of objects observed in OI emission would be useful both for studying the C/O ratio and also for hinting at the H_2O/CO abundance like in β Pictoris. The surprising discovery of significant quantities of molecular gas in debris disks is rapidly approaching a stage where we can draw conclusions about its role in late-stage planet formation and the composition of ices in distant solar systems.

SUMMARY POINTS

1. Summary point 1. These should be full sentences.
2. Summary point 2. These should be full sentences.
3. Summary point 3. These should be full sentences.
4. Summary point 4. These should be full sentences.

FUTURE ISSUES

1. Future issue 1. These should be full sentences.
2. Future issue 2. These should be full sentences.
3. Future issue 3. These should be full sentences.
4. Future issue 4. These should be full sentences.

DISCLOSURE STATEMENT

The authors are not aware of any affiliations, memberships, funding, or financial holdings that might be perceived as affecting the objectivity of this review.

ACKNOWLEDGMENTS

Acknowledgements, general annotations, funding.

LITERATURE CITED

Acke, B., Min, M., Dominik, C., et al. 2012, *Astron. Astrophys.*, 540, A125

Ahmic, M., Croll, B., & Artymowicz, P. 2009, *Apj. J.*, 705, 529

Alexander, R., Pascucci, I., Andrews, S., Armitage, P., & Cieza, L. 2014, Protostars and Planets VI, 475

ALMA Partnership, Brogan, C. L., Pérez, L. M., et al. 2015, *Apj. J. Lett.*, 808, L3

Apai, D., Schneider, G., Grady, C. A., et al. 2015, *Apj. J.*, 800, 136

Ardila, D. R., Golimowski, D. A., Krist, J. E., et al. 2004, *Apj. J. Lett.*, 617, L147

Artymowicz, P. 1997, Annual Review of Earth and Planetary *Science*s, 25, 175

Asensio-Torres, R., Janson, M., Hashimoto, J., et al. 2016, *Astron. Astrophys.*, 593, A73

Backman, D. E., & Paresce, F. 1993, in Protostars and Planets III, ed. E. H. Levy & J. I. Lunine, 1253–1304

Bailey, V., Meshkat, T., Reiter, M., et al. 2014, *Apj. J. Lett.*, 780, L4

Ballering, N. P., Rieke, G. H., Su, K. Y. L., & Montiel, E. 2013, *Apj. J.*, 775, 55

Ballering, N. P., Su, K. Y. L., Rieke, G. H., & Gáspár, A. 2016, *Apj. J.*, 823, 108

Ballesteros, F. J., Arnalte-Mur, P., Fernandez-Soto, A., & Martinez, V. J. 2017, ArXiv e-prints

Balog, Z., Kiss, L. L., Vinkó, J., et al. 2009, *Apj. J.*, 698, 1989

Barucci, M. A., Brown, M. E., Emery, J. P., & Merlin, F. 2008, Composition and Surface Properties of Transneptunian Objects and Centaurs, ed. M. A. Barucci, H. Boehnhardt, D. P. Cruikshank, A. Morbidelli, & R. Dotson, 143–160

Beichman, C. A., Bryden, G., Stapelfeldt, K. R., et al. 2006, *Apj. J.*, 652, 1674

Besla, G., & Wu, Y. 2007, *Apj. J.*, 655, 528

Beust, H., & Morbidelli, A. 1996, *Icarus*, 120, 358

Beust, H., Vidal-Madjar, A., Ferlet, R., & Lagrange-Henri, A. M. 1990, *Astron. Astrophys.*, 236, 202

Boccaletti, A., Thalmann, C., Lagrange, A.-M., et al. 2015, *Nature*, 526, 230

Boley, A. C., Payne, M. J., Corder, S., et al. 2012, *Apj. J. Lett.*, 750, L21

Bonnefoy, M., Milli, J., Ménard, F., et al. 2017, *Astron. Astrophys.*, 597, L7

Booth, M., Jordán, A., Casassus, S., et al. 2016, *MNRAS*, 460, L10

Booth, M., Dent, W. R. F., Jordán, A., et al. 2017, ArXiv e-prints

Boyajian, T. S., LaCourse, D. M., Rappaport, S. A., et al. 2016, *MNRAS*, 457, 3988

Brandeker, A., Liseau, R., Olofsson, G., & Fridlund, M. 2004, *Astron. Astrophys.*, 413, 681

Brandeker, A., Cataldi, G., Olofsson, G., et al. 2016, *Astron. Astrophys.*, 591, A27

Bryden, G., Beichman, C. A., Trilling, D. E., et al. 2006, *Apj. J.*, 636, 1098

Bryden, G., Beichman, C. A., Carpenter, J. M., et al. 2009, *Apj. J.*, 705, 1226

Buenzli, E., Thalmann, C., Vigan, A., et al. 2010, *Astron. Astrophys.*, 524, L1

Carmona, A., van den Ancker, M. E., Henning, T., et al. 2008, *Astron. Astrophys.*, 478, 795

Cataldi, G., Brandeker, A., Olofsson, G., et al. 2014, *Astron. Astrophys.*, 563, A66

Chauvin, G., Lagrange, A.-M., Beust, H., et al. 2012, *Astron. Astrophys.*, 542, A41

Chavez-Dagostino, M., Bertone, E., Cruz-Saenz de Miera, F., et al. 2016, *MNRAS*, 462, 2285

Chen, C. H., Mittal, T., Kuchner, M., et al. 2014, *Apj. J. Suppl.*, 211, 25

Chen, C. H., Li, A., Bohac, C., et al. 2007, *Apj. J.*, 666, 466

Chiang, E., & Fung, J. 2017, ArXiv e-prints

Chiang, E., Kite, E., Kalas, P., Graham, J. R., & Clampin, M. 2009, *Apj. J.*, 693, 734

Choquet, É., Milli, J., Wahhaj, Z., et al. 2017, *Apj. J. Lett.*, 834, L12

Corder, S., Carpenter, J. M., Sargent, A. I., et al. 2009, *Apj. J. Lett.*, 690, L65

Coulson, I. M., Walther, D. M., & Dent, W. R. F. 1998, *MNRAS*, 296, 934

Currie, T., Lisse, C. M., Kuchner, M., et al. 2015, *Apj. J. Lett.*, 807, L7

Currie, T., Lisse, C. M., Sicilia-Aguilar, A., Rieke, G. H., & Su, K. Y. L. 2011, *Apj. J.*, 734, 115

Currie, T., Rodigas, T. J., Debes, J., et al. 2012, *Apj. J.*, 757, 28

Currie, T., Guyon, O., Tamura, M., et al. 2017, *Apj. J. Lett.*, 836, L15

Czechowski, A., & Mann, I. 2007, *Apj. J.*, 660, 1541
Dawson, R. I., Murray-Clay, R. A., & Fabrycky, D. C. 2011, *Apj. J. Lett.*, 743, L17
de Vries, B. L., Acke, B., Blommaert, J. A. D. L., et al. 2012, *Nature*, 490, 74
Debes, J. H., Weinberger, A. J., & Kuchner, M. J. 2009, *Apj. J.*, 702, 318
Debes, J. H., Weinberger, A. J., & Schneider, G. 2008a, *Apj. J. Lett.*, 673, L191
Debes, J. H., Weinberger, A. J., & Song, I. 2008b, *Apj. J. Lett.*, 684, L41
Dent, W. R. F., Greaves, J. S., & Coulson, I. M. 2005, *MNRAS*, 359, 663
Dent, W. R. F., Wyatt, M. C., Roberge, A., et al. 2014, *Science*, 343, 1490
Dohnanyi, J. S. 1969, *Journ. Geophys. Res.*, 74, 2531
Donaldson, J. K., Lebreton, J., Roberge, A., Augereau, J.-C., & Krivov, A. V. 2013, *Apj. J.*, 772, 17
Draine, B. T. 2006, *Apj. J.*, 636, 1114
Draper, Z. H., Duchêne, G., Millar-Blanchaer, M. A., et al. 2016, *Apj. J.*, 826, 147
Eiroa, C., Fedele, D., Maldonado, J., et al. 2010, *Astron. Astrophys.*, 518, L131
Eiroa, C., Marshall, J. P., Mora, A., et al. 2013, *Astron. Astrophys.*, 555, A11
Eiroa, C., Rebollido, I., Montesinos, B., et al. 2016, *Astron. Astrophys.*, 594, L1
Ercolano, B., & Pascucci, I. 2017, Royal Society Open *Science*, 4, 170114
Ertel, S., Wolf, S., & Rodmann, J. 2012, *Astron. Astrophys.*, 544, A61
Ertel, S., Absil, O., Defrère, D., et al. 2014, *Astron. Astrophys.*, 570, A128
Ertel, S., Defrère, D., Absil, O., et al. 2016, *Astron. Astrophys.*, 595, A44
Espaillat, C. C., Ribas, Á., McClure, M. K., et al. 2017, *Apj. J.*, 844, 60
Esposito, T. M., Fitzgerald, M. P., Graham, J. R., & Kalas, P. 2014, *Apj. J.*, 780, 25
Esposito, T. M., Fitzgerald, M. P., Graham, J. R., et al. 2016, *Astron. J.*, 152, 85
Farihi, J. 2016, *New Astron. Rev.*, 71, 9
Feldt, M., Olofsson, J., Boccaletti, A., et al. 2017, *Astron. Astrophys.*, 601, A7
Fernández, R., Brandeker, A., & Wu, Y. 2006, *Apj. J.*, 643, 509
Fitzgerald, M. P., Kalas, P. G., & Graham, J. R. 2007, *Apj. J.*, 670, 557
Flaherty, K. M., Hughes, A. M., Andrews, S. M., et al. 2016, *Apj. J.*, 818, 97
France, K., Roberge, A., Lupu, R. E., Redfield, S., & Feldman, P. D. 2007, *Apj. J.*, 668, 1174
Fressin, F., Torres, G., Charbonneau, D., et al. 2013, *Apj. J.*, 766, 81
Gaidos, E. 2017, *MNRAS*, 470, L1
Galicher, R., Rameau, J., Bonnefoy, M., et al. 2014, *Astron. Astrophys.*, 565, L4
Gáspár, A., Psaltis, D., Rieke, G. H., & Özel, F. 2012, *Apj. J.*, 754, 74
Geiler, F., & Krivov, A. V. 2017, *MNRAS*, 468, 959
Golimowski, D. A., Ardila, D. R., Krist, J. E., et al. 2006, *Astron. J.*, 131, 3109
Goto, M., Geballe, T. R., McCall, B. J., et al. 2005, *Apj. J.*, 629, 865
Goździewski, K., & Migaszewski, C. 2014, *MNRAS*, 440, 3140
Graham, J. R., Kalas, P. G., & Matthews, B. C. 2007, *Apj. J.*, 654, 595
Greaves, J. S., Coulson, I. M., & Holland, W. S. 2000, *MNRAS*, 312, L1
Greaves, J. S., Holland, W. S., Wyatt, M. C., et al. 2005, *Apj. J. Lett.*, 619, L187
Greaves, J. S., Sibthorpe, B., Acke, B., et al. 2014, *Apj. J. Lett.*, 791, L11
Greaves, J. S., Holland, W. S., Matthews, B. C., et al. 2016, *MNRAS*, 461, 3910
Grigorieva, A., Thébault, P., Artymowicz, P., & Brandeker, A. 2007, *Astron. Astrophys.*, 475, 755
Hadamcik, E., Renard, J.-B., Rietmeijer, F. J. M., et al. 2007, *Icarus*, 190, 660
Hales, A. S., De Gregorio-Monsalvo, I., Montesinos, B., et al. 2014, *Astron. J.*, 148, 47
Hanner, M. S., & Newburn, R. L. 1989, *Astron. J.*, 97, 254
Hardy, A., Caceres, C., Schreiber, M. R., et al. 2015, *Astron. Astrophys.*, 583, A66
Heap, S. R., Lindler, D. J., Lanz, T. M., et al. 2000, *Apj. J.*, 539, 435
Hedman, M. M., & Stark, C. C. 2015, *Apj. J.*, 811, 67
Henyey, L. G., & Greenstein, J. L. 1941, *Apj. J.*, 93, 70
Higuchi, A. E., Sato, A., Tsukagoshi, T., et al. 2017, *Apj. J. Lett.*, 839, L14

Hines, D. C., Schneider, G., Hollenbach, D., et al. 2007, *Apj. J. Lett.*, 671, L165
Hobbs, L. M., Vidal-Madjar, A., Ferlet, R., Albert, C. E., & Gry, C. 1985, *Apj. J. Lett.*, 293, L29
Holland, W. S., Greaves, J. S., Zuckerman, B., et al. 1998, *Nature*, 392, 788
Holland, W. S., Matthews, B. C., Kennedy, G. M., et al. 2017, ArXiv e-prints
Hughes, A. M., Wilner, D. J., Andrews, S. M., et al. 2011, *Apj. J.*, 740, 38
Hughes, A. M., Wilner, D. J., Kamp, I., & Hogerheijde, M. R. 2008, *Apj. J.*, 681, 626
Hughes, A. M., Wilner, D. J., Mason, B., et al. 2012, *Apj. J.*, 750, 82
Hughes, A. M., Lieman-Sifry, J., Flaherty, K. M., et al. 2017, *Apj. J.*, 839, 86
Jackson, A. P., Wyatt, M. C., Bonsor, A., & Veras, D. 2014, *MNRAS*, 440, 3757
Jílková, L., & Portegies Zwart, S. 2015, *MNRAS*, 451, 804
Johnson, B. C., Lisse, C. M., Chen, C. H., et al. 2012, *Apj. J.*, 761, 45
Jura, M., Malkan, M., White, R., et al. 1998, *Apj. J.*, 505, 897
Kalas, P., Graham, J. R., & Clampin, M. 2005, *Nature*, 435, 1067
Kalas, P., Graham, J. R., Fitzgerald, M. P., & Clampin, M. 2013, *Apj. J.*, 775, 56
Kalas, P., & Jewitt, D. 1995, *Astron. J.*, 110, 794
Kalas, P., Graham, J. R., Chiang, E., et al. 2008, *Science*, 322, 1345
Kalas, P. G., Rajan, A., Wang, J. J., et al. 2015, *Apj. J.*, 814, 32
Kasper, M., Apai, D., Wagner, K., & Robberto, M. 2015, *Apj. J. Lett.*, 812, L33
Kennedy, G. M., & Wyatt, M. C. 2010, *MNRAS*, 405, 1253
—. 2012, *MNRAS*, 426, 91
—. 2014, *MNRAS*, 444, 3164
Kennedy, G. M., Wyatt, M. C., Bryden, G., Wittenmyer, R., & Sibthorpe, B. 2013, *MNRAS*, 436, 898
Kennedy, G. M., Matrà, L., Marmier, M., et al. 2015, *MNRAS*, 449, 3121
Kenworthy, M. A., & Mamajek, E. E. 2015, *Apj. J.*, 800, 126
Kenworthy, M. A., Lacour, S., Kraus, A., et al. 2015, *MNRAS*, 446, 411
Kenyon, S. J., & Bromley, B. C. 2002, *Astron. J.*, 123, 1757
—. 2008, *Apj. J. Suppl.*, 179, 451
Kenyon, S. J., Najita, J. R., & Bromley, B. C. 2016, *Apj. J.*, 831, 8
Kiefer, F., Lecavelier des Etangs, A., Augereau, J.-C., et al. 2014a, *Astron. Astrophys.*, 561, L10
—. 2014b, *Astron. Astrophys.*, 561, L10
Kiefer, F., Lecavelier des Etangs, A., Boissier, J., et al. 2014c, *Nature*, 514, 462
Kirchschlager, F., Wolf, S., Krivov, A. V., Mutschke, H., & Brunngräber, R. 2017, *MNRAS*, 467, 1614
Koerner, D. W., Sargent, A. I., & Ostroff, N. A. 2001, *Apj. J. Lett.*, 560, L181
Köhler, M., Mann, I., & Li, A. 2008, *Apj. J. Lett.*, 686, L95
Konishi, M., Grady, C. A., Schneider, G., et al. 2016, *Apj. J. Lett.*, 818, L23
Konopacky, Q. M., Marois, C., Macintosh, B. A., et al. 2016a, *Astron. J.*, 152, 28
Konopacky, Q. M., Rameau, J., Duchêne, G., et al. 2016b, *Apj. J. Lett.*, 829, L4
Kóspál, Á., Ardila, D. R., Moór, A., & Ábrahám, P. 2009, *Apj. J. Lett.*, 700, L73
Kóspál, Á., Moór, A., Juhász, A., et al. 2013, *Apj. J.*, 776, 77
Kral, Q., Clarke, C., & Wyatt, M. 2017a, ArXiv e-prints
Kral, Q., Matra, L., Wyatt, M., & Kennedy, G. 2017b, ArXiv e-prints
Kral, Q., Thébault, P., Augereau, J.-C., Boccaletti, A., & Charnoz, S. 2015, *Astron. Astrophys.*, 573, A39
Kral, Q., Wyatt, M., Carswell, R. F., et al. 2016, *MNRAS*, 461, 845
Kral, Q., Krivov, A. V., Defrere, D., et al. 2017c, ArXiv e-prints
Krist, J. E., Stapelfeldt, K. R., Bryden, G., & Plavchan, P. 2012, *Astron. J.*, 144, 45
Krist, J. E., Stapelfeldt, K. R., Golimowski, D. A., et al. 2005, *Astron. J.*, 130, 2778
Krist, J. E., Stapelfeldt, K. R., Bryden, G., et al. 2010, *Astron. J.*, 140, 1051
Krivov, A. V., Reidemeister, M., Fiedler, S., Löhne, T., & Neuhäuser, R. 2011, *MNRAS*, 418, L15

Kuchner, M. J., & Seager, S. 2005, ArXiv Astrophysics e-prints
Kuchner, M. J., & Stark, C. C. 2010, *Astron. J.*, 140, 1007
Lagrange, A.-M., Gratadour, D., Chauvin, G., et al. 2009, *Astron. Astrophys.*, 493, L21
Lagrange, A.-M., Bonnefoy, M., Chauvin, G., et al. 2010, *Science*, 329, 57
Lagrange, A.-M., Boccaletti, A., Milli, J., et al. 2012, *Astron. Astrophys.*, 542, A40
Lagrange, A.-M., Langlois, M., Gratton, R., et al. 2016, *Astron. Astrophys.*, 586, L8
Lamy, P. L., & Perrin, J.-M. 1986, *Astron. Astrophys.*, 163, 269
Le Bouquin, J.-B., Absil, O., Benisty, M., et al. 2009, *Astron. Astrophys.*, 498, L41
Lebreton, J., Beichman, C., Bryden, G., et al. 2016, *Apj. J.*, 817, 165
Lebreton, J., Augereau, J.-C., Thi, W.-F., et al. 2012, *Astron. Astrophys.*, 539, A17
Lee, E. J., & Chiang, E. 2016, *Apj. J.*, 827, 125
Leinert, C., Link, H., Pitz, E., & Giese, R. H. 1976, *Astron. Astrophys.*, 47, 221
Leinhardt, Z. M., & Stewart, S. T. 2012, *Apj. J.*, 745, 79
Lestrade, J.-F., & Thilliez, E. 2015, *Astron. Astrophys.*, 576, A72
Lestrade, J.-F., Matthews, B. C., Sibthorpe, B., et al. 2012, *Astron. Astrophys.*, 548, A86
Li, D., Telesco, C. M., & Wright, C. M. 2012, *Apj. J.*, 759, 81
Li, Z.-Y., Banerjee, R., Pudritz, R. E., et al. 2014, Protostars and Planets VI, 173
Lieman-Sifry, J., Hughes, A. M., Carpenter, J. M., et al. 2016, *Apj. J.*, 828, 25
Liou, J.-C., & Zook, H. A. 1999, *Astron. J.*, 118, 580
Liseau, R., Eiroa, C., Fedele, D., et al. 2010, *Astron. Astrophys.*, 518, L132
Lisse, C. M., Chen, C. H., Wyatt, M. C., et al. 2009, *Apj. J.*, 701, 2019
Lisse, C. M., Sitko, M. L., Marengo, M., et al. 2017, ArXiv e-prints
Lisse, C. M., Wyatt, M. C., Chen, C. H., et al. 2012, *Apj. J.*, 747, 93
Lomax, J. R., Wisniewski, J. P., Roberge, A., et al. 2017, ArXiv e-prints
Lyra, W., & Kuchner, M. 2013, *Nature*, 499, 184
MacGregor, M. A., Lawler, S. M., Wilner, D. J., et al. 2016a, *Apj. J.*, 828, 113
MacGregor, M. A., Wilner, D. J., Andrews, S. M., & Hughes, A. M. 2015a, *Apj. J.*, 801, 59
MacGregor, M. A., Wilner, D. J., Andrews, S. M., Lestrade, J.-F., & Maddison, S. 2015b, *Apj. J.*, 809, 47
MacGregor, M. A., Wilner, D. J., Rosenfeld, K. A., et al. 2013, *Apj. J. Lett.*, 762, L21
MacGregor, M. A., Wilner, D. J., Chandler, C., et al. 2016b, *Apj. J.*, 823, 79
MacGregor, M. A., Matra, L., Kalas, P., et al. 2017, ArXiv e-prints
Malamut, C., Redfield, S., Linsky, J. L., Wood, B. E., & Ayres, T. R. 2014, *Apj. J.*, 787, 75
Maldonado, J., Eiroa, C., Villaver, E., Montesinos, B., & Mora, A. 2012, *Astron. Astrophys.*, 541, A40
—. 2015, *Astron. Astrophys.*, 579, A20
Maldonado, R. F., Chavez, M., Bertone, E., & Cruz-Saenz de Miera, F. 2017, ArXiv e-prints
Malhotra, R. 1998, in Astronomical Society of the Pacific Conference Series, Vol. 149, Solar System Formation and Evolution, ed. D. Lazzaro, R. Vieira Martins, S. Ferraz-Mello, & J. Fernandez, 37
Mamajek, E. E., Quillen, A. C., Pecaut, M. J., et al. 2012, *Astron. J.*, 143, 72
Maness, H. L., Fitzgerald, M. P., Paladini, R., et al. 2008, *Apj. J. Lett.*, 686, L25
Maness, H. L., Kalas, P., Peek, K. M. G., et al. 2009, *Apj. J.*, 707, 1098
Marino, S., Wyatt, M. C., Kennedy, G. M., et al. 2017, ArXiv e-prints
Marino, S., Matrà, L., Stark, C., et al. 2016, *MNRAS*, 460, 2933
Marois, C., Macintosh, B., Barman, T., et al. 2008, *Science*, 322, 1348
Marshall, J. P., Moro-Martín, A., Eiroa, C., et al. 2014, *Astron. Astrophys.*, 565, A15
Mathews, G. S., Pinte, C., Duchêne, G., Williams, J. P., & Ménard, F. 2013, *Astron. Astrophys.*, 558, A66
Matrà, L., Panić, O., Wyatt, M. C., & Dent, W. R. F. 2015, *MNRAS*, 447, 3936
Matrà, L., MacGregor, M. A., Kalas, P., et al. 2017a, ArXiv e-prints

Matrà, L., Dent, W. R. F., Wyatt, M. C., et al. 2017b, *MNRAS*, 464, 1415
Matthews, B., Kennedy, G., Sibthorpe, B., et al. 2014a, *Apj. J.*, 780, 97
Matthews, B. C., Krivov, A. V., Wyatt, M. C., Bryden, G., & Eiroa, C. 2014b, Protostars and Planets VI, 521
Mazoyer, J., Boccaletti, A., Augereau, J.-C., et al. 2014, *Astron. Astrophys.*, 569, A29
McCabe, C., Duchêne, G., & Ghez, A. M. 2002, *Apj. J.*, 575, 974
Melis, C., Zuckerman, B., Rhee, J. H., et al. 2012, *Nature*, 487, 74
Meng, H. Y. A., Rieke, G. H., Su, K. Y. L., et al. 2012, *Apj. J. Lett.*, 751, L17
Meng, H. Y. A., Su, K. Y. L., Rieke, G. H., et al. 2014, *Science*, 345, 1032
—. 2015, *Apj. J.*, 805, 77
Mennesson, B., Millan-Gabet, R., Serabyn, E., et al. 2014, *Apj. J.*, 797, 119
Miles, B. E., Roberge, A., & Welsh, B. 2016, *Apj. J.*, 824, 126
Millan-Gabet, R., Serabyn, E., Mennesson, B., et al. 2011, *Apj. J.*, 734, 67
Millar-Blanchaer, M. A., Wang, J. J., Kalas, P., et al. 2016, *Astron. J.*, 152, 128
Milli, J., Hibon, P., Christiaens, V., et al. 2017a, *Astron. Astrophys.*, 597, L2
Milli, J., Vigan, A., Mouillet, D., et al. 2017b, *Astron. Astrophys.*, 599, A108
Min, M., Rab, C., Woitke, P., Dominik, C., & Ménard, F. 2016, *Astron. Astrophys.*, 585, A13
Mittal, T., Chen, C. H., Jang-Condell, H., et al. 2015, *Apj. J.*, 798, 87
Montesinos, B., Eiroa, C., Krivov, A. V., et al. 2016, *Astron. Astrophys.*, 593, A51
Montet, B. T., & Simon, J. D. 2016, *Apj. J. Lett.*, 830, L39
Montgomery, S. L., & Welsh, B. Y. 2017, *MNRAS*, 468, L55
Moór, A., Kóspál, Á., Ábrahám, P., et al. 2016, *Apj. J.*, 826, 123
Moór, A., Ábrahám, P., Juhász, A., et al. 2011, *Apj. J. Lett.*, 740, L7
Moór, A., Juhász, A., Kóspál, Á., et al. 2013, *Apj. J. Lett.*, 777, L25
Moór, A., Henning, T., Juhász, A., et al. 2015, *Apj. J.*, 814, 42
Moore, A., & Quillen, A. C. 2013, *MNRAS*, 430, 320
Morales, F. Y., Bryden, G., Werner, M. W., & Stapelfeldt, K. R. 2016, *Apj. J.*, 831, 97
Morales, F. Y., Padgett, D. L., Bryden, G., Werner, M. W., & Furlan, E. 2012, *Apj. J.*, 757, 7
Morales, F. Y., Rieke, G. H., Werner, M. W., et al. 2011, *Apj. J. Lett.*, 730, L29
Morey, É., & Lestrade, J.-F. 2014, *Astron. Astrophys.*, 565, A58
Moro-Martín, A., Malhotra, R., Bryden, G., et al. 2010, *Apj. J.*, 717, 1123
Moro-Martín, A., Carpenter, J. M., Meyer, M. R., et al. 2007, *Apj. J.*, 658, 1312
Moro-Martín, A., Marshall, J. P., Kennedy, G., et al. 2015, *Apj. J.*, 801, 143
Morrison, S., & Malhotra, R. 2015, *Apj. J.*, 799, 41
Mustill, A. J., & Wyatt, M. C. 2009, *MNRAS*, 399, 1403
—. 2012, *MNRAS*, 419, 3074
Nesvold, E. R., & Kuchner, M. J. 2015a, *Apj. J.*, 815, 61
—. 2015b, *Apj. J.*, 798, 83
Nesvold, E. R., Kuchner, M. J., Rein, H., & Pan, M. 2013, *Apj. J.*, 777, 144
Nesvold, E. R., Naoz, S., & Fitzgerald, M. P. 2017, *Apj. J. Lett.*, 837, L6
Nesvold, E. R., Naoz, S., Vican, L., & Farr, W. M. 2016, *Apj. J.*, 826, 19
Nesvorný, D., Jenniskens, P., Levison, H. F., et al. 2010, *Apj. J.*, 713, 816
Nielsen, E. L., Liu, M. C., Wahhaj, Z., et al. 2014, *Apj. J.*, 794, 158
Nilsson, R., Brandeker, A., Olofsson, G., et al. 2012, *Astron. Astrophys.*, 544, A134
Nunez, P. D., Scott, N. J., Mennesson, B., et al. 2017, ArXiv e-prints
Olofsson, G., Liseau, R., & Brandeker, A. 2001, *Apj. J. Lett.*, 563, L77
Olofsson, J., Juhász, A., Henning, T., et al. 2012, *Astron. Astrophys.*, 547, C1
Olofsson, J., Samland, M., Avenhaus, H., et al. 2016, *Astron. Astrophys.*, 591, A108
Osten, R., Livio, M., Lubow, S., et al. 2013, *Apj. J. Lett.*, 765, L44
Ozernoy, L. M., Gorkavyi, N. N., Mather, J. C., & Taidakova, T. A. 2000, *Apj. J. Lett.*, 537, L147
Pan, M., Nesvold, E. R., & Kuchner, M. J. 2016, *Apj. J.*, 832, 81

Pan, M., & Schlichting, H. E. 2012, *Apj. J.*, 747, 113
Panić, O., van Dishoeck, E. F., Hogerheijde, M. R., et al. 2010, *Astron. Astrophys.*, 519, A110
Pawellek, N., & Krivov, A. V. 2015, *MNRAS*, 454, 3207
Pawellek, N., Krivov, A. V., Marshall, J. P., et al. 2014, *Apj. J.*, 792, 65
Péricaud, J., Di Folco, E., Dutrey, A., Guilloteau, S., & Piétu, V. 2017, *Astron. Astrophys.*, 600, A62
Perrin, M. D., Duchene, G., Millar-Blanchaer, M., et al. 2015, *Apj. J.*, 799, 182
Piétu, V., di Folco, E., Guilloteau, S., Gueth, F., & Cox, P. 2011, *Astron. Astrophys.*, 531, L2
Quillen, A. C. 2006, *MNRAS*, 372, L14
Quillen, A. C., Morbidelli, A., & Moore, A. 2007, *MNRAS*, 380, 1642
Rameau, J., Chauvin, G., Lagrange, A.-M., et al. 2013, *Apj. J. Lett.*, 779, L26
Rameau, J., Nielsen, E. L., De Rosa, R. J., et al. 2016, *Apj. J. Lett.*, 822, L29
Rappaport, S., Vanderburg, A., Jacobs, T., et al. 2017, ArXiv e-prints
Raymond, S. N., O'Brien, D. P., Morbidelli, A., & Kaib, N. A. 2009, *Icarus*, 203, 644
Raymond, S. N., Armitage, P. J., Moro-Martín, A., et al. 2012, *Astron. Astrophys.*, 541, A11
Redfield, S. 2007, *Apj. J. Lett.*, 656, L97
Ricarte, A., Moldvai, N., Hughes, A. M., et al. 2013, *Apj. J.*, 774, 80
Ricci, L., Carpenter, J. M., Fu, B., et al. 2015a, *Apj. J.*, 798, 124
Ricci, L., Maddison, S. T., Wilner, D., et al. 2015b, *Apj. J.*, 813, 138
Riviere-Marichalar, P., Barrado, D., Augereau, J.-C., et al. 2012, *Astron. Astrophys.*, 546, L8
Riviere-Marichalar, P., Barrado, D., Montesinos, B., et al. 2014, *Astron. Astrophys.*, 565, A68
Roberge, A., Feldman, P. D., Weinberger, A. J., Deleuil, M., & Bouret, J.-C. 2006, *Nature*, 441, 724
Roberge, A., Welsh, B. Y., Kamp, I., Weinberger, A. J., & Grady, C. A. 2014, *Apj. J. Lett.*, 796, L11
Roberge, A., Chen, C. H., Millan-Gabet, R., et al. 2012, *Publ. Astron. Soc. Pac.*, 124, 799
Roberge, A., Kamp, I., Montesinos, B., et al. 2013, *Apj. J.*, 771, 69
Rodigas, T. J., Malhotra, R., & Hinz, P. M. 2014, *Apj. J.*, 780, 65
Rodigas, T. J., Hinz, P. M., Leisenring, J., et al. 2012, *Apj. J.*, 752, 57
Rodigas, T. J., Stark, C. C., Weinberger, A., et al. 2015, *Apj. J.*, 798, 96
Rodriguez, D. R., Duchêne, G., Tom, H., et al. 2015, *MNRAS*, 449, 3160
Sai, S., Itoh, Y., Fukagawa, M., Shibai, H., & Sumi, T. 2015, *Publ. Astron. Soc. Jap.*, 67, 20
Schleicher, D. G., Millis, R. L., & Birch, P. V. 1998, *Icarus*, 132, 397
Schneider, G., Silverstone, M. D., Hines, D. C., et al. 2006, *Apj. J.*, 650, 414
Schneider, G., Grady, C. A., Hines, D. C., et al. 2014, *Astron. J.*, 148, 59
Schneider, G., Grady, C. A., Stark, C. C., et al. 2016, *Astron. J.*, 152, 64
Schüppler, C., Löhne, T., Krivov, A. V., et al. 2015, *Astron. Astrophys.*, 581, A97
Sezestre, É., Augereau, J.-C., Boccaletti, A., & Thébault, P. 2017, ArXiv e-prints
Shannon, A., Bonsor, A., Kral, Q., & Matthews, E. 2016, *MNRAS*, 462, L116
Shannon, A., Mustill, A. J., & Wyatt, M. 2015, *MNRAS*, 448, 684
Shen, Y., Draine, B. T., & Johnson, E. T. 2009, *Apj. J.*, 696, 2126
Shu, F. H., Adams, F. C., & Lizano, S. 1987, *Annu. Rev. Astron. Astrophys.*, 25, 23
Sibthorpe, B., Kennedy, G. M., Wyatt, M. C., et al. 2017, *MNRAS*
Sierchio, J. M., Rieke, G. H., Su, K. Y. L., & Gáspár, A. 2014, *Apj. J.*, 785, 33
Slettebak, A. 1975, *Apj. J.*, 197, 137
Smith, B. A., & Terrile, R. J. 1984, *Science*, 226, 1421
Smith, R., Wyatt, M. C., & Haniff, C. A. 2009, *Astron. Astrophys.*, 503, 265
Soummer, R., Perrin, M. D., Pueyo, L., et al. 2014, *Apj. J. Lett.*, 786, L23
Stark, C. C., Schneider, G., Weinberger, A. J., et al. 2014, *Apj. J.*, 789, 58
Stewart, S. T., & Leinhardt, Z. M. 2012, *Apj. J.*, 751, 32
Strubbe, L. E., & Chiang, E. I. 2006, *Apj. J.*, 648, 652

Su, K. Y. L., Morrison, S., Malhotra, R., et al. 2015, *Apj. J.*, 799, 146
Su, K. Y. L., Rieke, G. H., Misselt, K. A., et al. 2005, *Apj. J.*, 628, 487
Su, K. Y. L., Rieke, G. H., Stapelfeldt, K. R., et al. 2009, *Apj. J.*, 705, 314
Takeuchi, T., & Artymowicz, P. 2001, *Apj. J.*, 557, 990
Tamura, M., Fukagawa, M., Kimura, H., et al. 2006, *Apj. J.*, 641, 1172
Tazaki, R., Tanaka, H., Okuzumi, S., Kataoka, A., & Nomura, H. 2016, *Apj. J.*, 823, 70
Thalmann, C., Janson, M., Buenzli, E., et al. 2011, *Apj. J. Lett.*, 743, L6
Thébault, P. 2009, *Astron. Astrophys.*, 505, 1269
Thébault, P., & Augereau, J.-C. 2007, *Astron. Astrophys.*, 472, 169
Thebault, P., Kral, Q., & Ertel, S. 2012, *Astron. Astrophys.*, 547, A92
Thi, W.-F., Pinte, C., Pantin, E., et al. 2014, *Astron. Astrophys.*, 561, A50
Thureau, N. D., Greaves, J. S., Matthews, B. C., et al. 2014, *MNRAS*, 445, 2558
Trilling, D. E., Bryden, G., Beichman, C. A., et al. 2008, *Apj. J.*, 674, 1086
van Lieshout, R., Dominik, C., Kama, M., & Min, M. 2014, *Astron. Astrophys.*, 571, A51
van Werkhoven, T. I. M., Kenworthy, M. A., & Mamajek, E. E. 2014, *MNRAS*, 441, 2845
Vandenbussche, B., Sibthorpe, B., Acke, B., et al. 2010, *Astron. Astrophys.*, 518, L133
Veras, D. 2016, Royal Society Open *Science*, 3, 150571
Visser, R., van Dishoeck, E. F., & Black, J. H. 2009, *Astron. Astrophys.*, 503, 323
Vitense, C., Krivov, A. V., Kobayashi, H., & Löhne, T. 2012, *Astron. Astrophys.*, 540, A30
Wang, J. J., Graham, J. R., Pueyo, L., et al. 2015, *Apj. J. Lett.*, 811, L19
—. 2016, *Astron. J.*, 152, 97
Welsh, B. Y., & Montgomery, S. L. 2015, Advances in Astronomy, 2015, 980323
White, J. A., Boley, A. C., Hughes, A. M., et al. 2016, *Apj. J.*, 829, 6
Williams, J. P., & Cieza, L. A. 2011, *Annu. Rev. Astron. Astrophys.*, 49, 67
Williams, J. P., Najita, J., Liu, M. C., et al. 2004, *Apj. J.*, 604, 414
Wilner, D. J., Andrews, S. M., MacGregor, M. A., & Hughes, A. M. 2012, *Apj. J. Lett.*, 749, L27
Wilner, D. J., Holman, M. J., Kuchner, M. J., & Ho, P. T. P. 2002, *Apj. J. Lett.*, 569, L115
Wilson, P. A., Lecavelier des Etangs, A., Vidal-Madjar, A., et al. 2017, *Astron. Astrophys.*, 599, A75
Wilson, T. L., Nilsson, R., Chen, C. H., et al. 2016, *Apj. J.*, 826, 165
Wittenmyer, R. A., & Marshall, J. P. 2015, *Astron. J.*, 149, 86
Wright, D. J., Chené, A.-N., De Cat, P., et al. 2011, *Apj. J. Lett.*, 728, L20
Wright, J. T., & Sigurdsson, S. 2016, *Apj. J. Lett.*, 829, L3
Wu, Y.-L., Close, L. M., Bailey, V. P., et al. 2016, *Apj. J.*, 823, 24
Wyatt, M. C. 2006, *Apj. J.*, 639, 1153
—. 2008, *Annu. Rev. Astron. Astrophys.*, 46, 339
Wyatt, M. C., & Dent, W. R. F. 2002, *MNRAS*, 334, 589
Wyatt, M. C., Dermott, S. F., Telesco, C. M., et al. 1999, *Apj. J.*, 527, 918
Wyatt, M. C., Panić, O., Kennedy, G. M., & Matrà, L. 2015, *Astrophys. Space Sci.*, 357, 103
Wyatt, M. C., Smith, R., Su, K. Y. L., et al. 2007, *Apj. J.*, 663, 365
Wyatt, M. C., Kennedy, G., Sibthorpe, B., et al. 2012, *MNRAS*, 424, 1206
Xie, J.-W., Brandeker, A., & Wu, Y. 2013, *Apj. J.*, 762, 114
Yamashita, T., Handa, T., Omodaka, T., et al. 1993, *Apj. J. Lett.*, 402, L65
Zubko, E., Muinonen, K., Videen, G., & Kiselev, N. N. 2014, *MNRAS*, 440, 2928
Zuckerman, B., Forveille, T., & Kastner, J. H. 1995, *Nature*, 373, 494
Zuckerman, B., & Song, I. 2012, *Apj. J.*, 758, 77